Journal of Geophysical Research: Atmospheres

RESEARCH ARTICLE
10.1029/2017JD028235

Key Points:
- Comparison of the spectra of halos and elves produced by different CG and IC lightning
- We have quantified the chemical impact of halos and elves; their contribution to global atmospheric chemistry is negligible
- The local production of NO and N_2O by halos and elves in the lower ionosphere and upper mesosphere is nonnegligible

Supporting Information:
- Supporting Information S1
- Table S1

Correspondence to:
F. J. Pérez-Invernón,
fjpi@iaa.es

Citation:
Pérez-Invernón, F. J., Luque, A., & Gordillo-Vázquez, F. J. (2018). Modeling the chemical impact and the optical emissions produced by lightning-induced electromagnetic fields in the upper atmosphere: The case of halos and elves triggered by different lightning discharges. *Journal of Geophysical Research: Atmospheres*, *123*, 7615–7641. https://doi.org/10.1029/2017JD028235

Received 22 DEC 2017
Accepted 8 JUN 2018
Accepted article online 19 JUN 2018
Published online 20 JUL 2018

Modeling the Chemical Impact and the Optical Emissions Produced by Lightning-Induced Electromagnetic Fields in the Upper Atmosphere: The case of Halos and Elves Triggered by Different Lightning Discharges

F. J. Pérez-Invernón[1], **A. Luque**[1], **and F. J. Gordillo-Vázquez**[1]

[1] Instituto de Astrofísica de Andalucía, CSIC, Granada, Spain

Abstract Halos and elves are transient luminous events produced in the lower ionosphere as a consequence of lightning-driven electromagnetic fields. These events can influence the upper atmospheric chemistry and produce optical emissions. We have developed different two-dimensional self-consistent models that couple electrodynamical equations with a chemical scheme to simulate halos and elves produced by vertical cloud-to-ground lightning discharges, compact intracloud discharges and energetic in-cloud pulses. The optical emissions from radiative relaxation of excited states of molecular and atomic nitrogen and oxygen have been calculated. We have upgraded previous local models of halos and elves to calculate for the first time the vibrationally detailed optical spectra of elves triggered by compact intracloud discharges and energetic in-cloud pulses. According to our results, the optical spectra of elves do not depend on the type of parent lightning discharge. Finally, we have quantified the local chemical impact in the upper atmosphere of single halos and elves. In the case of the halo, we follow the cascade of chemical reactions triggered by the lightning-produced electric field during a long-time simulation of up to 1 s. We obtain a production rate of NO molecules by single halos and elves of 10^{16} and 10^{14} molecules/J, respectively. The results of these local models have been used to estimate the global production of NO by halos and elves in the upper atmosphere at $\sim 10^{-7}$ Tg N/year. This global chemical impact of halos and elves is 7 orders of magnitude below the production of NO in the troposphere by lightning discharges.

Plain Language Summary Lightning discharges can trigger transient luminous events in the mesosphere. Halos and elves, two types of transient luminous events, are seen as red colored discs or rings at altitudes between 70 and 90 km. These luminous events are a consequence of a cascade of chemical reactions triggered by the lightning-produced electromagnetic field. In this paper, we develop two self-consistent models to investigate the inception and evolution of halos and elves produced by different types of lightning discharges. These models allow us to quantify the predicted chemical impact of halos and elves in the mesosphere as well as to predict their rovibrational optical spectra. Finally, we estimate the global production of NO by these events.

1. Introduction

Electromagnetic fields generated by lightning discharges produce transient luminous events (TLEs) in the lower ionosphere, as first proposed by Wilson (1925) and later detected by Franz et al. (1990). The local chemical impact and optical signature of these events have been investigated by many authors (Gordillo-Vázquez, 2008, 2010; Gordillo-Vázquez et al., 2011, 2012; Kuo et al., 2007; Parra-Rojas, Luque, & Gordillo-Vázquez, 2013; Parra-Rojas et al., 2015; Sentman et al., 2008; Winkler & Notholt, 2015). Some recent estimations suggest a future enhancement in the lightning activity as a consequence of the global temperature increase (Romps et al., 2014). Therefore, the study of the chemical influence of electric discharge processes in the atmosphere emerges as an important field in the characterization of the future atmosphere. Models and observations are needed to quantify the impact of these events.

Based on the physical production mechanism, TLEs can be categorized into elves, halos, sprites, blue jets, or gigantic jets (Pasko et al., 2012). Halos and sprites are a direct consequence of the quasi-electrostatic field created by lightning discharges (Pasko et al., 2012), while elves (emission of light and very low frequency

perturbations due to electromagnetic pulse sources), discovered by Fukunishi et al. (1996), are very fast TLEs produced by the interaction between lower ionospheric electrons and lightning-emitted electromagnetic pulses (EMPs).

In this paper, we will focus on halos and elves. Halos are glow discharges usually produced at altitudes between 75 and 80 km when the reduced electric field created by lightning discharges reaches the breakdown value of ~120 Td (Barrington-Leigh et al., 2001; Bering et al., 2002; Luque & Gordillo-Vázquez, 2011a; Moudry et al., 2003; Wescott et al., 2001). When the electric field becomes larger than the breakdown value, the electron-driven ionization rate of air molecules becomes larger than the attachment rate, causing a high increase in the electron density. Halos are usually seen accompanying a sprite, another kind of TLE formed by a complex structure of streamers. Some observations of single halos have been reported (Kuo et al., 2013; Marshall et al., 2006). The optical emissions from halos usually last between 1 and 3 ms. This kind of TLE is usually associated with negative or positive cloud-to-ground (CG) lightning discharges (Bering et al., 2002; Bering, Bhusal, et al., 2004; Bering, Benbrook, et al., 2004; Frey et al., 2007), since the return stroke stage of the CG lightning can transfer more total charge than intracloud or cloud-to-cloud lightning discharges (Maggio et al., 2009; Rakov & Uman, 2003).

Elves are very fast optical emissions (less than 1 ms) as a consequence of the heating of electron produced by lightning-generated EMPs (Inan et al., 1991, 1997; Moudry et al., 2003). This type of TLE is usually observed in a thin layer of the upper atmosphere usually located at 88 km of altitude (van der Velde & Montanyà, 2016), with a radius of more than 200 km. Lightning detection networks associate most of observed elves with CG lightning discharges, whose electromagnetic emission pattern produces toroidal light emissions in the lower ionosphere (Moudry et al., 2003; van der Velde & Montanyà, 2016).

The first observation of elves from spacecraft was accomplished by the Space Shuttle (Boeck et al., 1992). Other space missions, such as ISUAL (Chang et al., 2010) and JEM-GLIMS (Adachi et al., 2016), have investigated the optical signature of elves, mainly recording photons from the first and second positive systems of the molecular nitrogen (FP system of N_2 and the SP system of N_2), first negative system of the molecular nitrogen ion (N_2^+-1N), Meinel band of the molecular nitrogen ion (Meinel N_2^+), and Lyman-Birge-Hopfield (LBH) band of the molecular neutral nitrogen. In addition, ground-based observations have provided accurate information about the altitude and structure of elves (van der Velde & Montanyà, 2016). Moreover, some authors have previously investigated elves by modeling the impact of EMPs in the lower ionosphere (Inan et al., 1991; Kuo et al., 2007; Marshall, 2012; Marshall et al., 2010; Taranenko et al., 1993).

Recent investigations have also related elves with compact intracloud discharges (CIDs) (Marshall et al., 2015) and energetic in-cloud pulses (EIPs) (Liu et al., 2017). These kind of events are very fast and powerful discharges, first reported by Le Vine (1980), producing high electric field enhancements recorded some tens of kilometers away. Although the mechanism behind these events is not fully understood, some models explain the electromagnetic signals related to these types of lightning discharges by coupling of relativistic runaway electron avalanche and extensive atmospheric shower of cosmic rays with strong localized electric fields (Gurevich et al., 2004; Gurevich & Zybin, 2001; Watson & Marshall, 2007). The total charge moment change (CMC) produced by CIDs and EIPs is too low (below 3 C km; Karunarathne et al., 2016) to trigger halos or sprites. However, the pulses originated by both CIDs and EIPs can produce elves doublets after reflection with the ground surface, as previously studied by Marshall et al. (2015) and Liu et al. (2017). Lu et al. (2010) proposed the study of these events to confirm or discard their relation with terrestrial gamma-ray flashes (TGFs).

The detailed study of the chemical impact of halos and elves and their relation with the parent lightning discharge is still an open research topic. In the near future, two space-based missions will be devoted to the study of TLEs. The Atmosphere-Space Interactions Monitor (Neubert et al., 2006) of the European Space Agency was successfully launched on 2 April 2018 to observe TLEs from the International Space Station. In addition, the Tool for the Analysis of RAdiations from lightNIngs and Sprites (Blanc et al., 2007) mission of the Centre National d'Études Spatiales will be launched in 2019. Both Atmosphere-Space Interactions Monitor and Tool for the Analysis of RAdiations from lightNIngs and Sprites are equipped with TGF detectors and with high-temporal resolution photometers capable of recording optical signals from TLEs.

In this paper, we contribute to the knowledge of TLEs by modeling the inception and evolution of halos and elves using two different electrodynamical models that share the same set of kinetic reactions. On the one hand, we develop a self-consistent 2-D model of lightning-produced quasi-electrostatic fields coupled with

the kinetic scheme to simulate the local chemical signature produced by halos triggered by vertical CG lightning discharges. This halo model is based on the same scheme proposed by Pasko et al. (1995) and continued by other authors (Liu et al., 2015; Luque & Ebert, 2009; Kabirzadeh et al., 2015, 2017; Neubert et al., 2011; Pérez-Invernón, Gordillo-Vázquez, & Luque, 2016; Pérez-Invernón, Luque, & Gordillo-Vázquez, 2016; Qin et al., 2014). We have contributed to the upgrade of these models by adding a more detailed chemical scheme and extending the chemical simulations up to times of 1 s after the onset of the halo. On the other hand, we have developed a self-consistent finite-difference time domain (FDTD) model of electromagnetic wave propagation that has also been coupled with the kinetic scheme to simulate elves produced by vertical CG lightning discharges, CIDs and EIPs. This FDTD model is based on the one proposed by Inan et al. (1991) and later on upgraded by other authors (Kuo et al., 2007; Marshall, 2012; Marshall et al., 2010; Taranenko et al., 1993). Marshall et al. (2015) and Liu et al. (2017) investigated the elves triggered by impulsive in-cloud discharges, such as CIDs and EIPs, using a basic chemical scheme. In this work, we use a similar FDTD scheme to simulate the electrodynamic of elves coupled with a detailed set of chemical reactions. This approach has allowed us to compare the spectra of different types of lightning generated very impulsive TLE.

In section 2 we describe the developed models, their implementation for different source currents, and the method to compute the synthetic spectra of the predicted TLEs. In section 3 we present and discuss the results of our calculations. We quantify the chemical influence of halos in the atmosphere and compare the calculated spectra of each simulated TLE. Finally, we conclude in section 5 summing up the most important implications of the results obtained.

2. Models

In section 2.1 we describe the kinetic scheme that determines the local chemical impact and optical emissions due to halos and elves. The detailed electrodynamical model developed for each case is detailed in sections 2.2 and 2.3

2.1. Kinetic Scheme

The kinetic scheme determines the interaction between particles, as well as electron mobility and diffusion in the presence of a reduced electric field. We use a kinetic scheme with 136 species interacting through 1,076 chemical reactions. The complete set of chemical reactions is detailed in the supporting information (Albritton, 1978; Bates, 1988; Biondi et al., 1971; Borst & Zipf, 1970; Brasseur & Solomon, 1986; Cacciatore et al., 2005; Calo et al., 1971; Capitelli et al., 2000; Cartwright et al., 1977; Castillo et al., 2004; Dagdigian et al., 1988; Erdman & Zipf, 1987; Gilmore et al., 1992; Gordiets et al., 1995; Gordillo-Vázquez, 2008, 2010; Gudmundsson et al., 2001; Guerra & Loureiro, 1999; Herron & Green, 2001; Kam & Pipkin, 1991; Kamaratos, 2006; Kazil et al., 2003; Kossyi et al., 1992; Krupenie, 1972; Kurnosov et al., 2007; Laher & Gilmore, 1990; Lawton & Phelps, 1978; Lepoutre et al., 1977; Linstrom & Mallard, 2015; Makhlouf et al., 1995; Morrill, 2000; Morrill & Benesch, 1996; Pagnon et al., 1995; Pancheshnyi, 2013; Parra-Rojas, Luque, & Gordillo-Vázquez, 2013; Parra-Rojas et al., 2015; Peverall et al., 2001; Phelps, 1991, 2005, 2008; Piper, 1988, 1992, 1989; Piper et al., 1985; Pitchford et al., 2012; Radzig & Smirnov, 2012; Rodríguez et al., 1991; Sentman et al., 2008; Simek, 2002, 2003; Skalni et al., 1996; Slanger & Copeland, 2003; Smirnov & Massey, 1982; Starikovskaia et al., 2001; Thoman et al., 1992; Turnbull & Lowe, 1991; Vallance Jones, 1974; Viggiano, 2006; Whitaker et al., 1981; Yaron et al., 1976; Zinn et al., 1990). The main reaction types in terms of the chemical and optical impact produced by TLEs are

1. Electron impact excitation of neutral species given by

$$e + A \rightarrow e + A^{*}, \tag{1}$$

   and ionization given by

$$e + A \rightarrow 2e + A^{+}, \tag{2}$$

   where the species A can be N_2, O_2, N, O, NO, N_2O, O_3, or CO_2. The species A^* can be electronically and/or vibrationally excited in the case of N_2, while only electron excitation is considered for the rest of the species. A^+ stands for the positive ion of the molecule or atom A. The cross sections used to calculate these reaction rates are detailed in the supporting information.
2. Electron attachment processes, among which the most important is the electron driven dissociative attachment of O_2 molecules,

$$e + O_2 \rightarrow O + O^{-}. \tag{3}$$

This attachment reaction rate dominates electron-ionization processes of N_2 and O_2 for reduced electric fields below the breakdown value. When the breakdown field is reached, ionization becomes larger than attachment, triggering a cascade of reactions that, ultimately, lead to the observation of TLEs.

3. Electron detachment processes. As previously studied by Luque and Gordillo-Vázquez (2011a) and Marshall (2012), some detachment processes like associative detachment of O^- by N_2 can dominate the production of electrons at electric fields below the breakdown value. We consider the electron detachment from negative ions by N_2 and O_2 described by Pancheshnyi (2013), which are electric field dependent. Furthermore, we include also electron detachment from O^- interacting with other important species, such as CO and NO (Biondi et al., 1971; Kossyi et al., 1992). However, according to Moruzzi et al. (1968), the electric field dependence of O^- + CO and O^- + NO detachment rates is negligible.
4. Electron-ion and ion-ion recombination processes, contributing to remove charge carriers (Gordillo-Vázquez, 2008; Parra-Rojas, Luque, & Gordillo-Vázquez, 2013; Parra-Rojas et al., 2015; Sentman et al., 2008).
5. Vibrational redistribution, energy pooling, vibrational-translational and vibrational-vibrational processes involving electronically and vibrationally excited molecules of N_2 (Gordillo-Vázquez, 2010).
6. Chemical reactions involving excited state species (Gordillo-Vázquez, 2008; Parra-Rojas, Luque, & Gordillo-Vázquez, 2013; Parra-Rojas et al., 2015; Sentman et al., 2008).
7. Positive and negative ion chemistry, in addition to ground state chemistry. These reactions contribute to the enhancement of some neutral species (Gordillo-Vázquez, 2008; Parra-Rojas, Luque, & Gordillo-Vázquez, 2013; Parra-Rojas et al., 2015; Sentman et al., 2008).
8. Odd hydrogen and odd nitrogen reactions (Sentman et al., 2008).
9. Radiative decay, electronic quenching, and vibrational quenching. These three processes compete to deexcitate molecules and atoms. Most important quenching reactions include N_2 and O_2. The most of the radiative decay constants and electronic and vibrational quenching rates used in this work are taken from Gordillo-Vázquez (2010). However, to the best of our knowledge, the electronic quenching rate of $N_2(E^3\Sigma_g^+)$ by N_2 or O_2 is not described in the literature. This process can be important to describe the vibrational distribution function (VDF) of the electrovibrationally excited molecule $N_2(C^3\Pi_u, v)$. As an approximation of the electronic quenching rate of $N_2(E^3\Sigma_g^+)$, we set its value equal to the quenching rate of the molecule $N_2(C^3\Pi_u, v = 0)$.

Mobility, diffusion, and some reaction coefficients contributing to species production and loss can also depend on the reduced electric field. These dependences are obtained by solving off-line the steady state Boltzmann equation for the gas mixture (humid air) using the package BOLSIG+ (Hagelaar & Pitchford, 2005).

We calculate the temporal evolution of the concentration of emitting atoms and molecules computing the total emitted photons per second according to the radiative processes. This kinetic scheme allows us to predict the existence or absence of halo optical emissions in some important spectral bands and lines, such as the nitrogen first (550–1200 nm) and second (250–450 nm) positive systems, nitrogen first negative line between the zero vibrational levels v' and v'' (391.4 nm), nitrogen LBH band (110–200 nm), molecular oxygen atmospheric (538–1,580 nm), Noxon (1,908 nm), and Herzberg I (243–488 nm) systems, atomic oxygen green (557 nm), red (630 nm), near infrared lines (777 and 844 nm), and other atomic and molecular emissions. We pay special attention to the vibrational chemistry of excited species such as $N_2(B^3\Pi_g, v = 0, \ldots, 6)$, $N_2(C^3\Pi_u, v = 0, \ldots, 4)$, and $N_2(a^1\Pi_g, v = 0, \ldots, 15)$. This detailed description of the vibrational levels of the mentioned excited species allows us to estimate their VDFs. The proposed kinetic scheme is also useful to predict the optical emission spectra of halos and elves corresponding to the first and second positive systems of molecular nitrogen, as well as to the LBH band. We collect the emission bands in the last column of Table 1.

Finally, we use the software QTPlaskin, developed by Luque (2011), to analyze the main processes that contribute to create or destroy each species as a function of time.

2.1.1. Optical Emissions

Let $N_i(\vec{r})$ be the spatial density distribution of one of the calculated species $N_2(B^3\Pi_g, v = 0, \ldots, 6)$, $N_2(C^3\Pi_u, v = 0, \ldots, 4)$, $N_2(a^1\Pi_g, v = 0, \ldots, 15)$, $NO(A^2\Sigma^+)$, $O_2(A^3\Pi_u^+)$, $O_2(b^1\Pi_g^+)$, $O_2(a^1\Delta_g)$, $O(^1S)$, $O(^1D)$, $O(^3P)$, or $O(^5P)$ and A_i the radiative decay constant of deexcitation and emission of photons at a given wavelength. The temporal

Table 1
Species Considered in the Chemical Scheme and Emission Bands

Neutrals	Negative charged particles	Positive charged particles	Emission bands
$N_2(X^1\Sigma_g^+, v = 0, \ldots, 10)$, $N_2(A^3\Sigma_u^+, v = 0, \ldots, 16)$,	e, O^-, O_2^-, O_3^-, O_4^-,	N^+, N_2^+, $N_2^+(B^2\Sigma_u^+)$, N_3^+,	FP and SP systems of N_2: (550–1,200 nm)
$N_2(B^3\Pi_g, v = 0, \ldots, 6)$, $N_2(C^3\Pi_u, v = 0, \ldots, 4)$,	NO^-, NO_2^-, NO_3^-,	N_4^+, O^+, O_2^+, O_4^+, NO^+,	and (250–450 nm)
$N_2(a^1\Pi_g, v = 0, \ldots, 15)$, $N_2(W^3\Delta_u, v = 0, \ldots, 3)$,	CO_3^-, CO_4^-	NO_2^+, N_2O^+, $N_2O_2^+$,	FNS of N_2^+ (391.4 nm)
$N_2(E^3\Sigma_g^+)$, $N_2(w^1\Delta_u)$, $N_2(a'^1\Sigma_u^-)$, $N_2(a''^1\Sigma_g^+)$,		N_2NO^+, O_2NO^+,	LBH band of N_2 (110–200 nm)
$N_2(B'^3\Sigma_u^-, v = 0, 1)$			Emissions from molecular oxygen
$NO(A^2\Sigma^+)$, N, $N(^2D)$, $N(^2P)$, O_2, $O_2(A^3\Pi_u^+)$,			(538–1,580 nm), (1,908 nm),
			and (243–488 nm)
$O_2(b^1\Pi_g^+)$, $O_2(a^1\Delta_g)$, O, $O(^1S)$, $O(^1D)$, $O(^3P)$,		$(H_2O)O_2^+$, $(H_2O)H^+$,	Noxon system (1,908 nm)
$O(^5P)$, O_3, CO, NO, NO_2, NO_3, N_2O, N_2O_5, H, OH,		$(H_2O)_2H^+$, $(H_2O)_3H^+$,	Herzberg I (243–488 nm) system
H^*, H_2O, HO_2, H_2O_2, HNO_3, CO_2, $CO_2(001)$,		$(H_2O)_4H^+$, $(H_2O)OHH^+$,	Emissions from atomic oxygen (557 nm),
$CO_2(100)$, $CO_2(010)$, $CO_2(02^00)$, $CO_2(02^20)$,			(630 nm), (777 nm), and (844 nm)
$CO_2(03^10)$, $CO_2(03^30)$, $CO_2(11^10)$			

Note. LBH = Lyman-Birge-Hopfield; FP = first positive; SP = second positive; FNS = first negative system.

evolution of the total number of emitted photons per second from each species can be calculated integrating in volume as

$$I = \int A_i N_i(\vec{r}) \mathrm{d}V. \tag{4}$$

The knowledge of these quantities together with the energy difference between levels allow us to build synthetic spectra. As a consequence of the low air density above TLEs, the observed spectra from spacecraft would be very similar to the spectra at the emitting source. However, if the spectrograph is located near the ground level, as in the case of the instrument *GRAnada Sprite Spectrograph and Polarimeter* (Gordillo-Vázquez et al., 2018; Passas et al., 2014, 2016), the effect of the atmospheric attenuation on each spectral transition has to be included in the calculation of the emitted spectra in order to compare with observed spectra.

We calculate the optical transmittance of the atmosphere between an emitting TLE and an observer located at a horizontal distance of 350 km using the software MODTRAN 5 (Berk et al., 2005). As can be seen in Figure 2 of Gordillo-Vázquez et al. (2012), the air transmittance dependence on the light frequency is irregular. We use a tool code previously developed in the study of Parra-Rojas, Passas, et al. (2013) to obtain the rovibronic bands of the FP system of N_2 system. This program is based on the calculation of the decay constant of each rovibrational level following the method described in Kovacs (1969) for triplet transitions. Afterward, the obtained transmittance for different altitudes can be applied to the emitted spectra to derive the predicted observed optical signature of halos and elves from ground-based spectrographs like GRAnada Sprite Spectrograph and Polarimeter (Passas et al., 2016).

2.2. Model of Halo Production

We model the impact of lightning-induced quasi-electrostatic fields in the lower ionosphere of the Earth using a cylindrically symmetrical scheme similar to the one used in previous models by, for example, Luque and Ebert (2009), Neubert et al. (2011), Liu et al. (2015), Qin et al. (2014), Pérez-Invernón, Gordillo-Vázquez, and Luque (2016) and Pérez-Invernón, Luque, and Gordillo-Vázquez (2016). The time evolution of the electric field is coupled with the transport of charged particles and with an extended set of chemical reactions.

Strokes produced by CG lightning discharges lower electric charge to the ground, accumulating the same amount of opposite sign charge at cloud altitudes. We model this charge accumulation as a sphere of radius 0.5 km at an altitude $h = 7$km (Maggio et al., 2009). The time evolution of the total accumulated charge is given by a biexponential function

$$\frac{\mathrm{d}Q(t)}{\mathrm{d}t} = I(t) = \frac{Q_{\max}}{\tau_1 - \tau_2}\left(\exp(-t/\tau_1) - \exp(-t/\tau_2)\right), \tag{5}$$

where $Q_{\max}$ is the opposite sign total charge lowered to the ground and where $\tau_1 = 1$ms and $\tau_2 = 0.1$ms, respectively, the total discharge time and the rise time of the discharge current. The CMC, given by the product $hQ_{\max}$, determines both the electric field imposed on the ionosphere and its strength.

Halos are a direct consequence of the lightning-induced quasi-electrostatic field. The shape of the optical emissions produced by a halo corresponds to the spatial distribution of the quasi-electrostatic field created right above a dipolar lightning discharge. In addition, the characteristic time of halos (several milliseconds) also agrees with the characteristic time of the quasi-electrostatic field. For this reason, we neglect the effect of the radiation field. The quasi-electrostatic field created by the charge resulting from equation (5) is calculated using FISHPACK (Sweet, 1977), a 2-D Poisson solver in cylindrical coordinates that solves the equation

$$\nabla^2 \phi = -\frac{\rho}{\epsilon_0}, \tag{6}$$

where ϕ is the electric potential, ϵ_0 is the permitivity of vacuum, and ρ is the charge density located in the integration domain. This quantity includes the lightning-accumulated charge in the troposphere as well as the induced charge in the mesosphere and lower ionosphere.

The resultant electric field induces electron and ion transport in the mesosphere and lower ionosphere, separating charges of opposite sign. The transport of the charged species i is determined by the advection-diffusion flux $\mathbf{\Phi}_i$, whose components in the vertical and radial directions (z and r) are given, in the case of electrons, by

$$\Phi_{e,z} = -D_e \frac{\partial N_e}{\partial z} - \mu_e E_z N_e \tag{7a}$$

$$\Phi_{e,r} = -D_e \frac{\partial N_e}{\partial r} - \mu_e E_r N_e, \tag{7b}$$

while in the case of ions we can neglect diffusion and write these equations as

$$\Phi_{i,z} = -v_{i,z} N_i, \tag{8a}$$

$$\Phi_{i,r} = -v_{i,r} N_i, \tag{8b}$$

where D_e, μ_e, and N_e are, respectively, the electron diffusion coefficient, mobility, and density, while v_i and N_i are the ion velocities and densities. The electron diffusion coefficient and mobility depend on the gas composition and the electric field and will be described in the next section. In the case of ions, the velocity of an ion with mass m_i under the influence of high reduced electric fields is given by (Fahr & Müller, 1967; Pancheshnyi, 2013)

$$v_i = \sqrt{\frac{2\theta_z}{\pi m_i}}, \tag{9}$$

where θ_z, the kinetic energy of the ion in the presence of an electric field E, is given by Fahr and Müller (1967) and Pancheshnyi (2013) as

$$\theta_z = q_e E \lambda, \tag{10}$$

where q_e is the negative elementary electric charge and λ is the mean free path of particles in the gas between successive collisions, calculated as a function of the air density N (Chapman & Cowling, 1970)

$$\lambda = \left(\sqrt{2}\pi d^2 N\right)^{-1}. \tag{11}$$

where d is the average diameter of molecules in air.

In the case of halos, where the quasi-electrostatic field remains high for several milliseconds, numerical oscillations can appear as a consequence of large density gradients. For this reason, equations (7) and (8) are solved using a Koren limiter function (Montijn et al., 2006) to obtain charged species fluxes. Then, we are able to write the continuity equation of the species i including kinetics and transport as

$$\frac{\partial N_{e,i}}{\partial t} + \nabla \cdot \mathbf{\Phi}_{e,i} = P_{e,i} - L_{e,i}, \tag{12}$$

where $P_{e,i}$ and $L_{e,i}$ are the production and loss rates of electrons or species i, determined by the kinetic scheme. We solve this equation using an explicit Runge-Kutta method of order 5 with step size control based on the Dormand and Prince algorithm (Dormand & Prince, 1980). We solve this equation for altitudes above 50 km, where the plasma density is important.

Equations (6)–(12) are discretized in a cylindrical grid with a spatial resolution given by Δz = 100 m and Δr = 500 m. We use an adaptive time step $\Delta t < 3 \times 10^{-6}$ s. For the Poisson equation (6), we use boundary conditions of the Neumann type at r = 300 km, undetermined in the axis of symmetry and of the Dirichlet type in the upper (ionosphere) and lower (ground) boundaries assuming that both of them behave as perfect electric conductors. In the case of the transport equations (7) and (8) we use Neumann type boundary conditions.

The quasi-electrostatic field produced by the discharge evolves influenced by the total transferred charge (5) roughly during the first millisecond. After that time, the lightning discharge ends and no more charge is deposited on the clouds. Therefore, the main change of the quasi-electrostatic field in the lower ionosphere is determined by the field-induced electron currents, with time scales approximately given by the dielectric relaxation time at each altitude level. Therefore, the time derivative of the quasi-electrostatic field will decrease progressively as the field is screened at higher altitudes. We take advantage of this fact and implement a method to progressively decrease the computational cost of our simulation. We include a parameter p in the code that calculates the maximum time derivative of the reduced electric field at a given time t′ by computing the difference between the field at that time and at the previous time step ($t' - \Delta t$):

$$p\left(t'\right) = \max\left(\frac{\partial\left(\frac{E(r,z,t')}{N(r,z)}\right)}{\partial t'}\right) = \max\left(\frac{\frac{E(r,z,t')-E(r,z,t'-\Delta t)}{N(r,z)}}{\Delta t}\right). \tag{13}$$

This parameter gives us the maximum absolute variation of the reduced electric field per second. Using p we can then estimate the total number of time steps n that are necessary to see a maximum absolute change of 0.1 Td as

$$n\Delta t = \frac{0.1}{p}. \tag{14}$$

If n is greater than 1, we deactivate the Poisson equation solver for that number of subsequent time steps, keeping the electric field and its effects constant. This allows us to exclusively solve the equations related to the chemistry and the charged particles transport assuming a maximum relative error in the electric field less than 0.1 Td.

2.3. Model of Elve Production

As mentioned in section 1, we have also developed a two-dimensional FDTD model of electromagnetic wave propagation coupled with a chemical scheme. This FDTD model solves the Maxwell equations in a 2-D grid domain (Inan et al., 1991; Inan & Marshall, 2011; Kuo et al., 2007; Liu et al., 2017; Luque et al., 2014; Marshall et al., 2015, 2010; Taranenko et al., 1993) to obtain the electric and magnetic field vectors **E** and **H** produced by lightning discharges (CG, CID, or EIP). In particular, the developed FDTD model is implemented in a cylindrical 2-D grid domain.The model uses a modified Ohm's equation to calculate the current density induced by the electric fields in the upper atmosphere (Lee & Kalluri, 1999; Luque et al., 2014). We couple the scheme of electromagnetic wave propagation with a set of continuity reactions, updating component densities n_i at each time step. The complete set of equations is given by

$$\nabla \times \mathbf{E} = -\mu_0 \frac{\partial \mathbf{H}}{\partial t}, \tag{15}$$

$$\nabla \times \mathbf{H} = \epsilon_0 \frac{\partial \mathbf{E}}{\partial t} + \mathbf{J}, \tag{16}$$

$$\frac{\mathrm{d}\mathbf{J}}{\mathrm{d}t} + \nu\mathbf{J} = \epsilon_0 \omega_p^2(\mathbf{r}, t)\mathbf{E} + \omega_b(\mathbf{r}, t) \times \mathbf{J}, \tag{17}$$

$$\frac{\partial N_i}{\partial t} = G_i - L_i. \tag{18}$$

We solve Maxwell equations (15) and (16), where ϵ_0 and μ_0 are the permitivity and permeability of free space, using a two-dimensional FDTD model in a cylindrical 2-D grid domain using the Yee algorithm (Yee, 1966) with a space step Δd shorter than the minimum characteristic wavelength of the source electric current in each case and with a time step shorter than $\Delta d/\sqrt{3}c$ (Inan & Marshall, 2011). The term **J** contains current densities, that is, the lightning channel current density and the electron current density induced by electric fields in the lower ionosphere. We impose absorbing boundary conditions using convolutional perfectly matched layers (Inan & Marshall, 2011). We define the ground as a perfect conductor.

The modified Ohm's equation (17) is solved using the same two-dimensional FDTD model as the Maxwell equations, as proposed by Lee and Kalluri (1999). Equation (17) is only solved at altitudes where the electron density becomes important. At these altitudes near the ionosphere, the electron conductivity is orders of magnitude higher than the ion conductivity, hence we neglect the ion current density contribution. We use the same notation as Lee and Kalluri (1999) and Luque et al. (2014), where $\nu = e/\mu m_e$ is the effective collision frequency between electrons and neutrals, dependent on electron charge magnitude e and mass m_e, and on electron mobility μ. The term $\omega_p = (e^2 n_e/m_e\epsilon_0)^{1/2}$ corresponds to the plasma frequency for electrons and depends on the electron density n_e. Finally, $\omega_b = e\mathbf{B}_0/m_e$ is the electron gyrofrequency, where $\mathbf{B}_0$ is the background magnetic field, considered zero in the two-dimensional approximation.

Marshall and Inan (2008), Marshall et al. (2010), and Marshall (2014) investigated the effect of the background magnetic field in the wave attenuation. The angle between the direction of wave propagation of lightning-radiated waves and the magnetic field vector, as shown by Marshall and Inan (2008), Marshall et al. (2010), and Marshall (2014). Considering that lightning-radiated waves are upward, the angle between their direction of propagation and the background magnetic field is determined by the geomagnetical latitude. As discussed by Marshall and Inan (2008), Marshall et al. (2010), and Marshall (2014), the effect of the geomagnetic field can be neglected for angles ranging between 0° and 45° but can be important for higher geomagnetic latitudes. As the occurrence of lightning is mostly gathered at tropical latitudes (Christian et al., 2003), we neglect the effect of the geomagnetic field. However, it is worth emphasizing that the propagation of the pulses and the subsequent elves would be different at higher geomagnetic latitudes (Marshall, 2014; Marshall & Inan, 2008; Marshall et al., 2010).

Equation (18) describes the evolution of each component's density as a function of its gains G_i and losses L_i. This equation will be particularized for each component and will be coupled with equations (15)–(17) as a consequence of the electric field dependence of some reaction rates. We solve this equation using a forward Euler method choosing a time step smaller than the dielectric relaxation time, the fastest chemical reaction characteristic time, and $\Delta d/\sqrt{3}c$.

Regarding the CG lightning discharge, we assume that the return stroke current follows a biexponential function (Rakov & Uman, 2003) of the form

$$I(t) = I_0\left(\exp(-t/\tau_1) - \exp(-t/\tau_2)\right), \tag{19}$$

where τ_2 is the rise time of the current wave and τ_1 is the total duration of the stroke. According to Rakov and Uman (2003), τ_2 and τ_1 have characteristic values of tens of microseconds and hundreds of microseconds, respectively. In this work, we set a risetime of 5μs and a total duration of the stroke of 50μs (Heidler et al., 1999).

We set a 7-km-long channel propagation velocity at 0.75 ×c, where c is the speed of light. The vertical source current density vector $\mathbf{J}(t)$ is obtained dividing the lightning current $I(t)$ by the lateral section of a cell. We have considered CG lightning discharges with current peaks of 154, 220, 275, and 440 kA (Rakov & Uman, 2003), respectively. According to Barrington-Leigh and Inan (1999), the lightning peak current threshold for the production of elves is about 60 kA, while new results suggest that this threshold is 88 kA (Blaes et al., 2016). The detection threshold for elves of the ISUAL instrument is estimated to be around 80 kA (Chern et al., 2014; Kuo et al., 2007).

In the case of elves triggered by CIDs located at 18 km of altitude, we set as source of EMP the lightning currents modeled by Watson and Marshall (2007). We use the Modified Transmission Line Exponential Increasing model proposed by Watson and Marshall (2007) for downward positive discharges, with a peak current of ∼400 kA (Cummer et al., 2014; Liu et al., 2017; Lyu et al., 2015). The EIP negative current source located at 13 km of altitude is taken from Liu et al. (2017), who simulated a EIP-driven elve produced by a current with a peak of ∼542 kA. As Liu et al. (2017) claims, this current could produce TGFs that could be detected by Fermi (Briggs et al., 2010; Cummer et al., 2014; Lyu et al., 2015).

After defining the atmosphere composition and the current source, we solve the system of equations (15)–(18) in a two-dimensional mesh where r corresponds to horizontal distances from the lightning discharge and z corresponds to altitude. Horizontal distances are between 0 and 550 km with a step of 0.5 km in the case of elves triggered by CG lightning discharges and between 0 and 250 km with a step of 0.1 km in the case of elves triggered by CID and EIPs. The altitude domain is between 0 and 97 km, with a vertical step of 0.1 km. We include 20-cell-wide absorbing boundaries. Equations (17) and (18) are exclusively

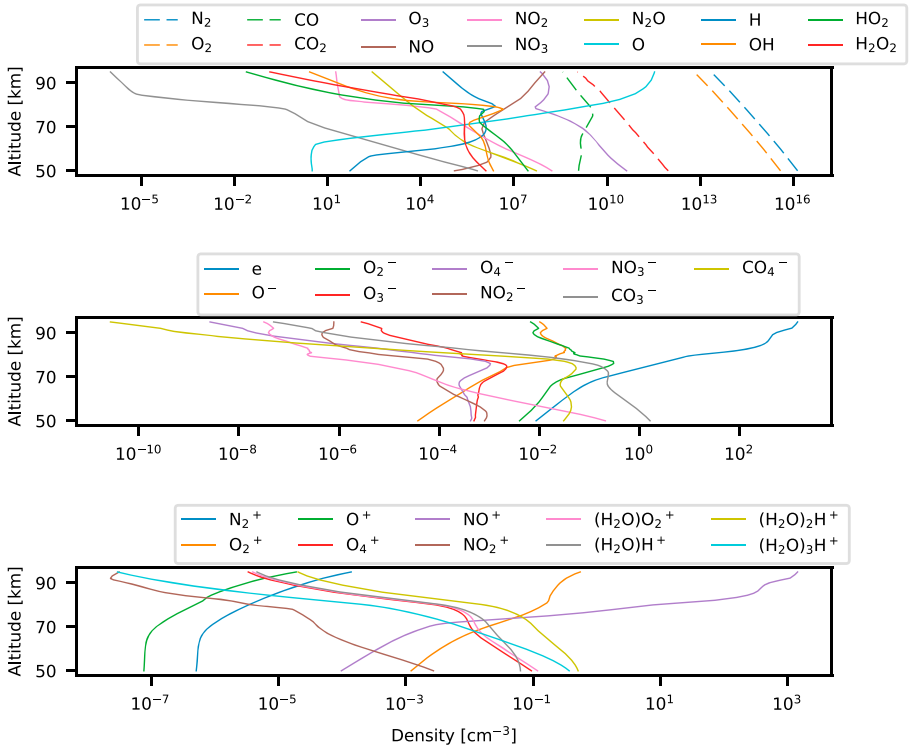

Figure 1. Most important species at equilibrium conditions. Dashed lines correspond to most abundant species. The H_2O density is set to 1.6×10^9 cm^{-3}.

solved in the region where electron density is important, that is, above 50 km of altitude. Regarding the time step, we set it to 10 ns, ensuring that the constrains detailed above are satisfied.

We have developed this method in several Fortran subroutines, compiling them to create Python modules. The code is parallelized with a shared-memory approach based on OpenMP. We run each parallelized simulation describing 1 ms of the evolution of the elve during a time of about one day using 12 CPUs.

2.4. Initial Conditions

As initial conditions, we use the air density profile and composition at nighttime conditions in November from the Whole Atmosphere Community Climate Model (Marsh et al., 2013) for a latitude of 38° and a longitude of 0°. We also use the electron density proposed by Hu et al. (2007). Then we relax the system for 6.5 s under the presence of cosmic ray ionization (Thomas, 1974) solving the continuity equation of each particle to obtain the equilibrium profiles associated to our model. The concentrations of N_2, O_2, CO, CO_2, and H_2O are assumed to be constant. Figure 1 shows the most important species at equilibrium conditions.

3. Results and Discussion

3.1. Halo Model Results

We apply the model described in section 2.2 to simulate the inception of halos and to quantify both their local chemical impact in the upper atmosphere and their optical signature.

Ionization, attachment, and other reaction rates have a nonlinear dependence with the reduced electric field. Due to this fact, the upper atmospheric chemical influence and optical emissions driven by lightning depend strongly on the CMC associated with the discharge. We investigate the effect of three different CG lightning discharges with CMCs of 140, 350, and 560 C km (Cummer & Lyons, 2004; Maggio et al., 2009; Marshall & Stolzenburg, 2001; Rakov & Uman, 2003). We also explore the *long* time (1 s) halo mesospheric chemistry for the last case.

3.1.1. Local Chemical Influence of Halos in the Mesosphere

Figure 2 shows the reduced electric field and the electron density in the upper atmosphere created by vertical CG lightning discharges with different CMCs. The reduced electric field reaches the breakdown value

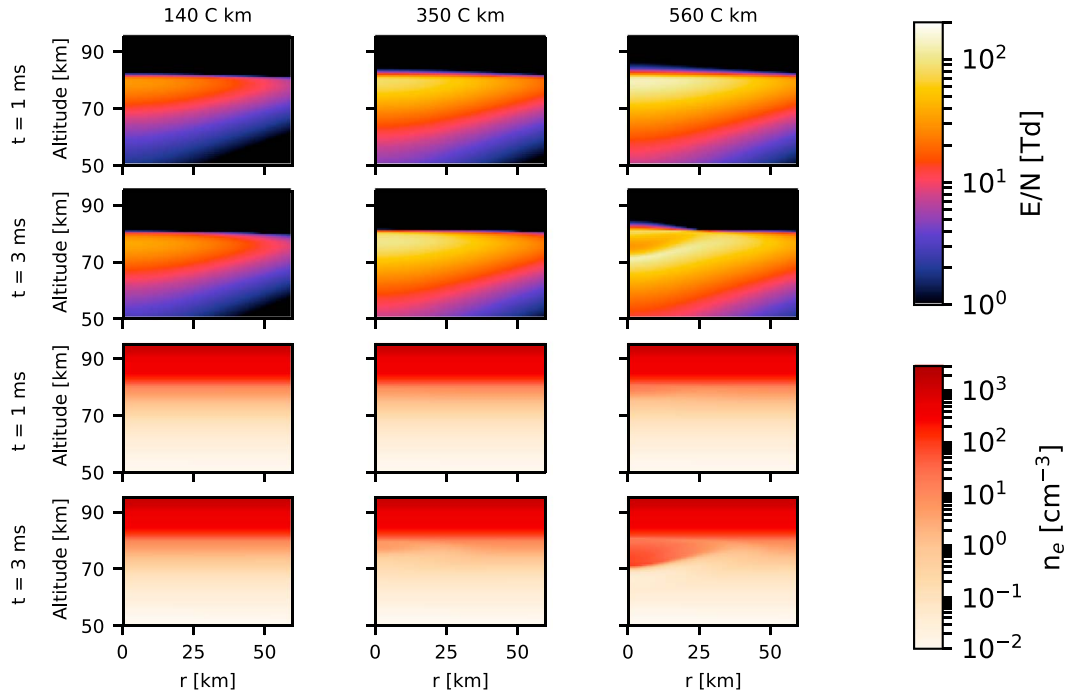

Figure 2. Reduced electric field and electron density in the upper atmosphere produced by three different vertical cloud-to-ground lightning discharges. The vertical axis corresponds to altitude in the atmosphere, while the horizontal axis represents the horizontal distance from the lightning discharge. The charge moment change value created by each discharge is 140, 350, and 560 C km. We show snapshots at 1 and 3 ms after the beginning of each discharge.

of ~120 Td (or $\sim 120 \times 10^{-17}$ V cm^2) in the case of the two most energetic discharges, increasing the electron density in the lower ionosphere at an altitude of ~80 km. Afterward, this enhancement of electrons triggered by ionization contributes to screen the electric field, as can be clearly seen in the case of a lightning discharge with a CMC of 560 C km.

Let us analyze now the chemical influence of halos focusing on each species. Figures 3 and 4 summarize the density variation of some of the main neutrals and ions in the atmosphere of the Earth. It can be seen that the main chemical effect of halos is focused at altitudes around 75 km. Furthermore, the horizontal chemical influence extends up to 20 km from the center of the halo.

The density of some initial ground state neutrals suffers an enhancement in the center of the halo 3 ms after its onset. The atomic nitrogen N, whose background concentration is negligible, increases by about 8.8×10^{21} molecules. The increase of N is followed by other species like O, N_2O, NO_2, and NO, with increases with respect to their ambient values of ~ 0.7%, ~ 0.2%, ~ 0.1%, and ~ 0.01%, respectively. The concentration of NO_x would increase after the extinction of this halo, as the produced N atoms will rapidly be converted into NO and NO_2 after interacting with O_2.

The main processes that contribute to enhance the densities of N and O are the collisions of electrons with N_2 and O_2, respectively. The enhancement in the density of N_2O is due to the associative detachment of O^- by N_2, while the increase of NO is influenced by processes that involve $N(^2D)$ and O_2. Finally, NO interacts with molecules containing O atoms to create NO_2.

3.1.2. Model Limitation: Possible Sprite Inception

Figure 5 shows the temporal evolution of the $N_2(C^3\Pi_u(v=0))$ density and the reduced electric field in a vertical column above two different discharges. For the weakest discharge, with a CMC of 140 C km, optical emissions due to $N_2(C^3\Pi_u(v=0))$ disappear around 4 ms after the beginning of the discharge, while the reduced electric field is too low to produce emissions or ionization below 75 km of altitude. However, for higher CMCs the reduced electric field is above the breakdown value at altitudes below 75 km. In that region, the lack of electrons entails a dielectric relaxation time ($\tau_m = \epsilon_0(en_e\mu_e)^{-1}$) of tens of milliseconds, resulting in a long-lasting halo that disagrees with observations (Kuo et al., 2013; Marshall et al., 2006). Probably, a sprite would appear

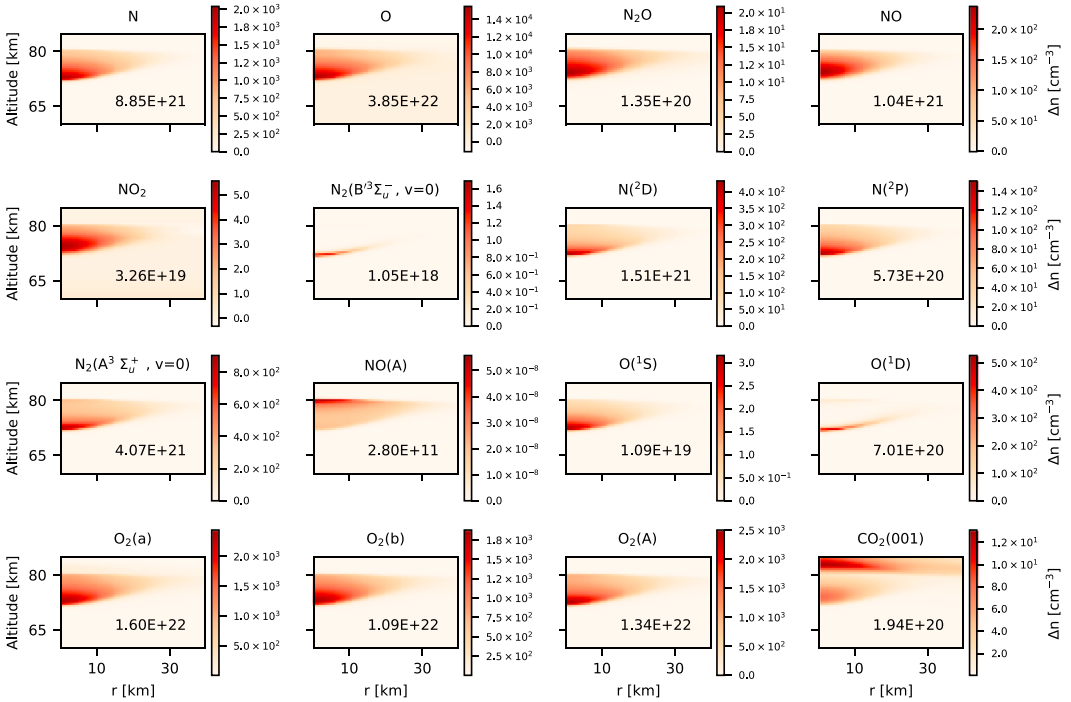

Figure 3. Variation (with respect to ambient values) of the density of some neutrals in the atmosphere of the Earth 3 ms after the beginning of a cloud-to-ground lightning discharge producing a charge moment change of 560 C km. The axes are the same as in Figure 2. We show the total number of molecules created by the halo in the lower right corner of each subplot.

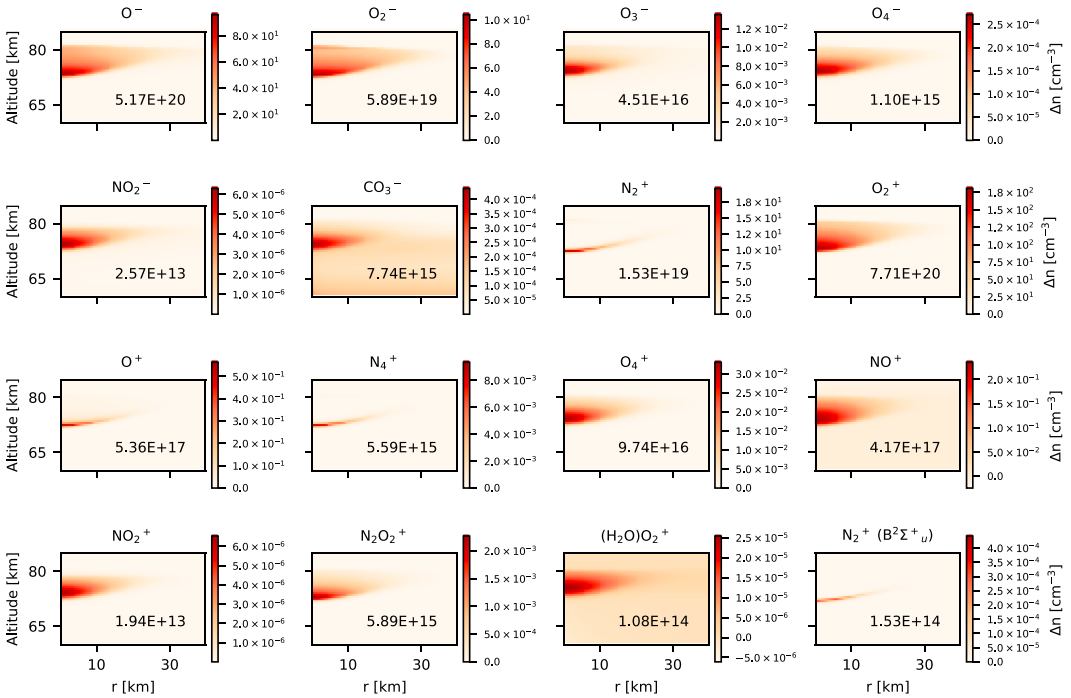

Figure 4. Density variation of some ions in the atmosphere of the Earth 3 ms after the onset of a cloud-to-ground lightning discharge producing a charge moment change of 560 C km. The axes are the same as in Figure 2. We show the total number of molecules created by the halo in the lower right corner of each subplot.

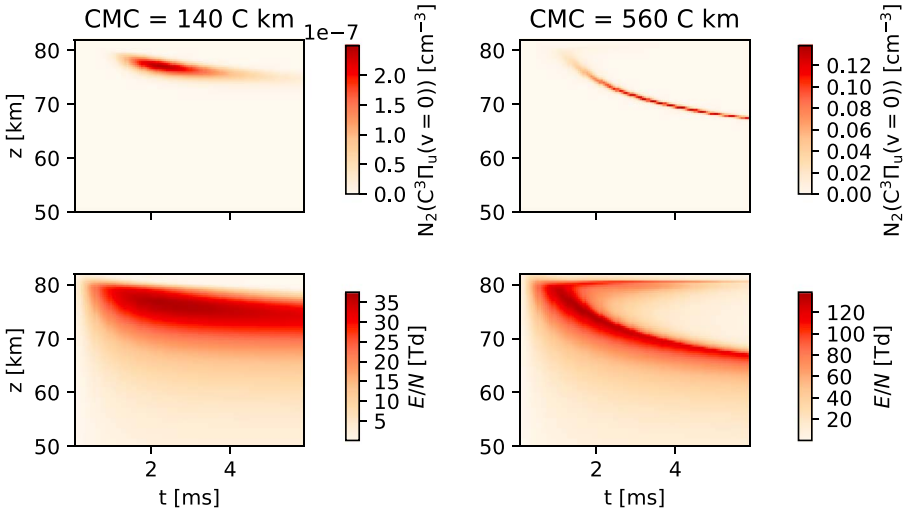

Figure 5. Temporal evolution of the density of the emitting species $N_2(C^3\Pi_u(v = 0))$ (top panels) and the reduced electric field (bottom panels) in a vertical column above the lightning discharge. Panels in the first and second columns correspond to two different lightning discharges with charge moment changes of 140and 560 C km, respectively.

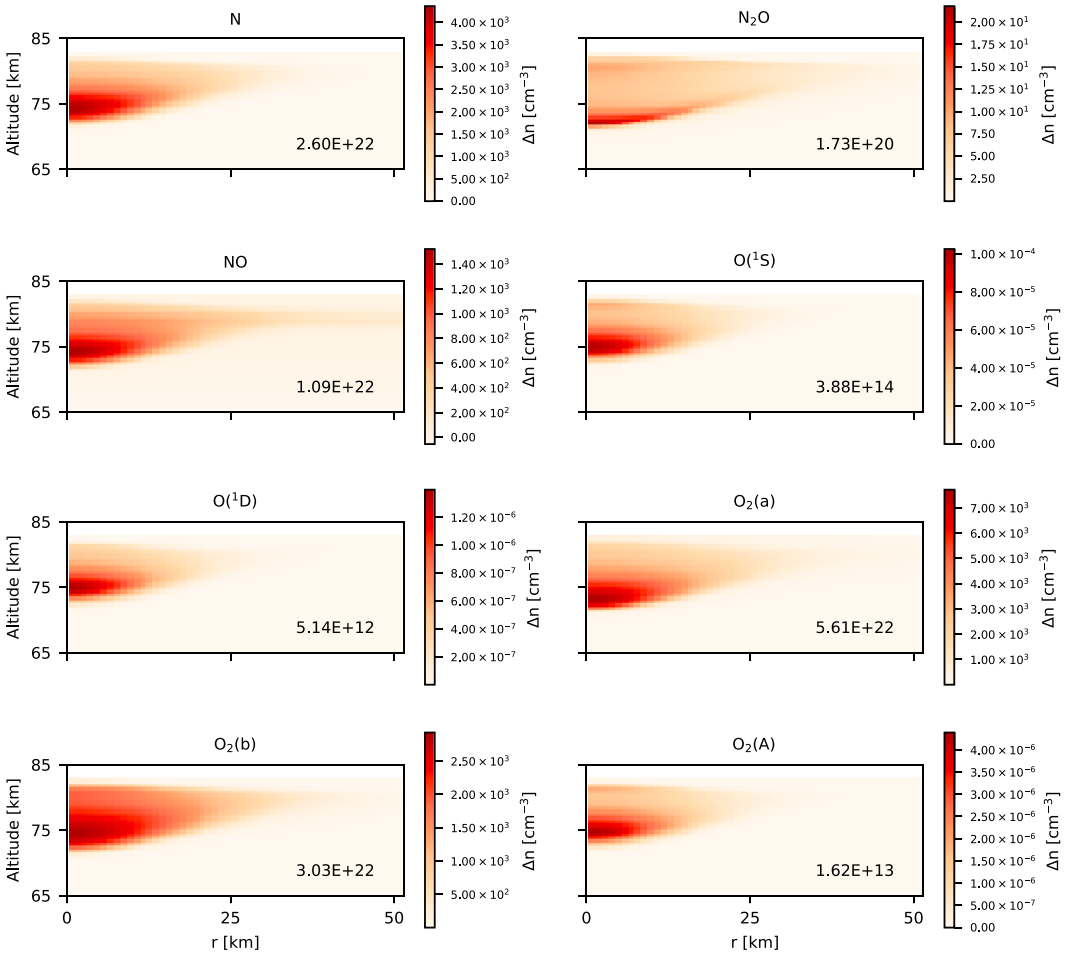

Figure 6. Variation of the density of some neutrals in the atmosphere of Earth 1 s after the beginning of a cloud-to-ground lightning discharge producing a charge moment change of 560 C km. The axes are the same as in Figure 2. We show the total number of molecules created by the halo in the lower right corner of each subplot.

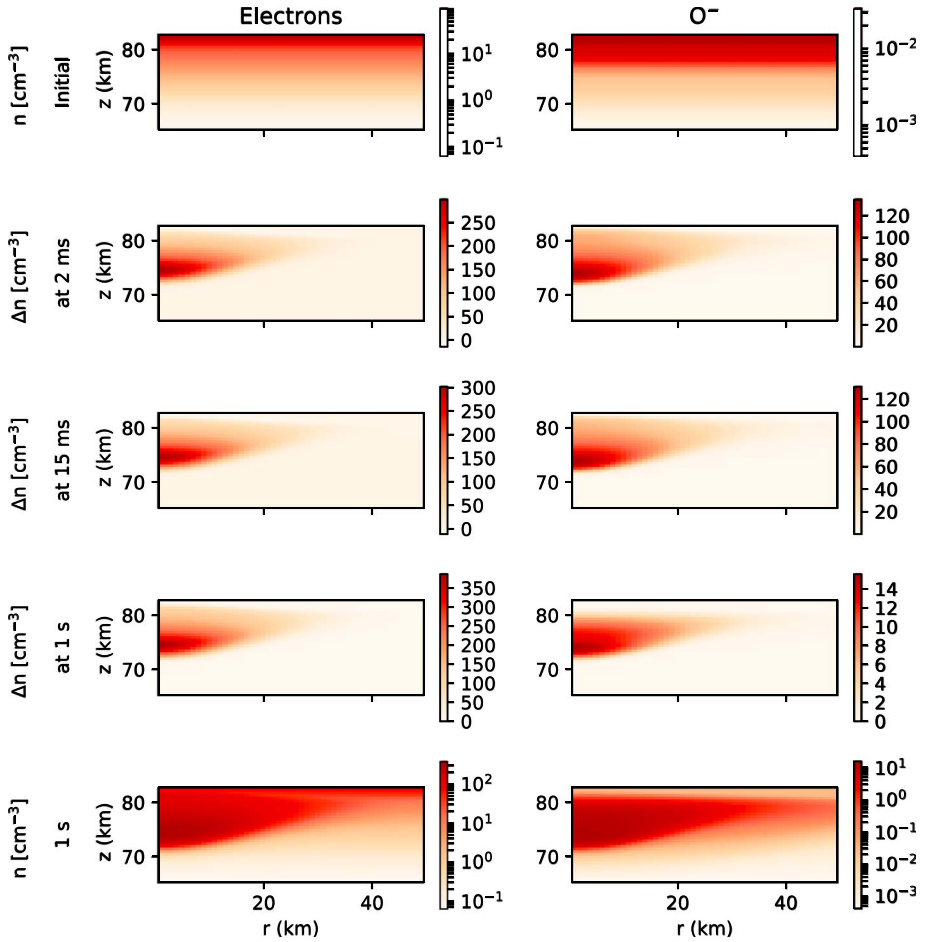

Figure 7. Evolution of the density of electrons and O^- in the atmosphere of the Earth during 1 s after the beginning of a cloud-to-ground lightning discharge producing a charge moment change of 560 C km. The axes are the same as in Figure 2. The first and last rows show the initial and final profiles, respectively. The second, third, and fourth rows show the increase in the density at different times since the beginning of the lightning discharge.

in this situation, screening the electric field below 75 km of altitude. However, our model is not capable of describing the evolution of sprite streamers.

3.1.3. Long-Time Halo Simulation

In section 3.1.2 we verified that the halo model fails for relatively long times (~6 ms) for lightning discharges producing a high CMC (~560 C km), as it cannot simulate the development and spreading of sprite streamers. However, Kuo et al. (2013) reported some luminous halos without sprite inception triggered by lightning discharges with large CMCs, greater than 800 C km. In this section we model halos produced by a lightning discharge that accumulates 80 C of charge during 1 ms, followed by another discharge that removes the accumulated charge in the next 5 ms. This approach allows us to avoid sprite inception. In addition, the hypothesis whereby the charge on clouds is removed by a subsequent discharge would explain the exceptional single halos reported by Kuo et al. (2013).

After the cloud charge removal, the only net charge present in the amosphere would be the sole halo-induced charge in the mesosphere. According to our simulation, these charges would produce a maximum reduced electric field of 13 Td, quite lower than the breakdown field. We neglect the effect of this field and deactivate both the Poisson solver and the transport of charged particle in order to accelerate the calculations. In addition, we decrease the spatial resolution. This allows us to extend the simulation to predict the local chemical influence of lightning discharges in the lower ionosphere up to the scale of seconds.

The most important variations in the density of neutrals 1 s after the halo onset are plotted in Figure 6. Although the increase of ground neutrals is more than 1 order of magnitude lower than background densities shown in Figure 1, it is interesting to note and quantify the enhancements of some important species,

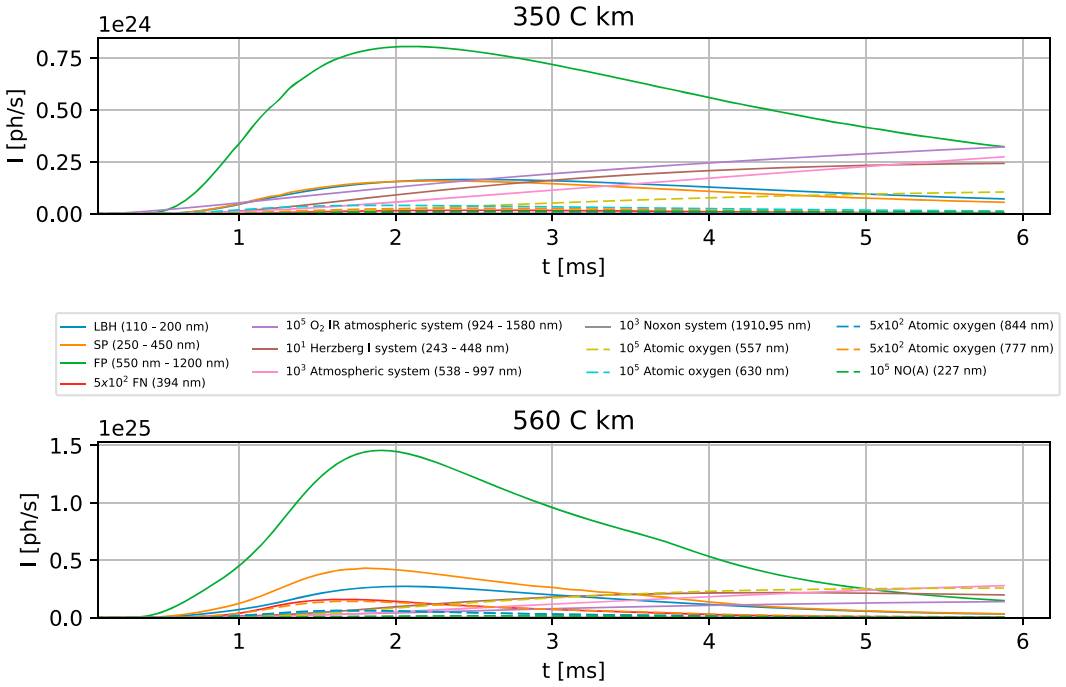

Figure 8. Temporal evolution of the total emitted photons per second (for the main spectral bands) from halos. This figure shows results for two halos triggered by two cloud-to-ground lightning discharges producing total charge moment changes of, respectively, 350 and 560 C km. As can be seen in the legend box, some lines have been multiplied by different factors in an effort to plot all of them together. LBH, SP, FP, and FN correspond to the Lyman-Birge-Hopfield band and second positive, first positive, and first negative systems of molecular nitrogen, respectively.

such as N_2O and NO. The increase of these species densities with respect to background in the center of the halo 1 s after its onset is of ~ 0.2% and ~ 0.1%, respectively. Despite the high relative enhancement of atomic nitrogen, the absolute increase is of the same order than NO, as can be seen in the number written in the first plot of Figure 6. We can compare Figures 3 and 6 to note that a long-time simulation produced a larger ratio of NO_x to N, as N is converted into NO_x. These results suggest that halos have a nonnegligible local and regional chemical influence in the upper atmosphere near thunderstorms. Arnone et al. (2008) obtained a local enhancement of NO_x produced by sprites streamers of 10% at 52 km of altitude, increasing up to 60 km. Therefore, we can conclude that the chemical influence of a halo is between 1 and 2 orders of magnitude below the influence of a sprite.

We can also estimate the energy deposited in the mesosphere by a halo. Our models calculate the total flux of electrons produced by the lightning-generated electric field. Given both the temporal evolution of the flux of electrons and the electric field, the power deposited in the mesosphere can be calculated as the product of these two quantities and the total volume of the halo. Finally, the total deposited energy can be estimated knowing the duration of the event. This calculation leads us to estimate that the total amount of energy deposited in the mesosphere is about 10^6 J. Therefore, the production rate of NO by a halo can be approximated in terms of energy as 10^{16} molecules of NO/J, 1 order of magnitude lower than the production rate of NO by lightning, estimated in 10^{17} molecules of NO/J (Price et al., 1997). The ISUAL instrument observations estimated an annual occurrence of TLEs about 1.2×10^7 (Chern et al., 2014). The 6% of the observed TLEs by ISUAL were halos. The computed production of NO molecules by a halo together with the observation of halo occurrence by ISUAL allow us to estimate the total amount of NO created by halos in 2×10^{-7} teragrams of nitrogen per year (Tg N/year). This value is quite below the estimated production of NO by lightning discharges, estimated between 5 and 9 Tg N/year (Nault et al., 2017; Schumann & Huntrieser, 2007). According to these numbers, the global chemical influence of halos is trivial.

It is also worth analyzing the temporal evolution of electrons up to 1 s. Figure 7 shows the evolution of the density of electrons and O^- in the atmosphere of the Earth. It can be seen how the O^- is transformed into

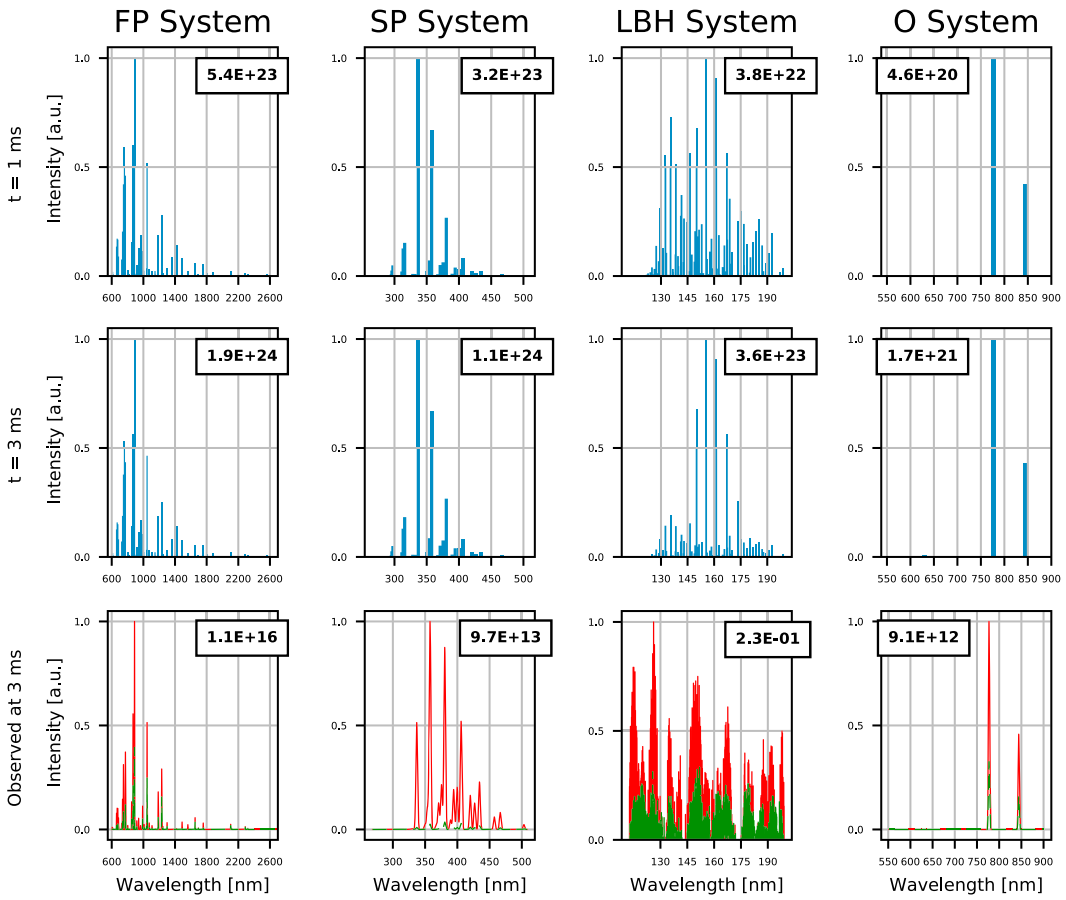

Figure 9. Calculated spectra of halos for different spectral bands. The first and the second rows show different moments of the emission spectra at the source, while the third row shows the predicted observed spectra at 3 km (red solid line) and 275 m (green dashed line) over the sea and at a horizontal distance of 350 km (between the halo and the observer) 3 ms after the onset of the lightning discharge. We plot the intensity of the bands in arbitrary units, normalizing each subplot to the stronger transition in each band. The numbers in boxes correspond to photons per second in the case of emisson spectra, and photons per second and squared meters in the case of the predicted observed spectra. FP = first positive; SP = second positive; LBH = Lyman-Birge-Hopfield band.

electrons between 15 ms and 1 s. The main chemical process that contributes to this transformation is the associative detachment reaction

$$O^- + CO \rightarrow e + CO_2, \tag{20}$$

that exceeds other associative detachment processes when the applied electric field is zero. However, at the very initial moment when the halo develops and the electric field is high, the rate of this reaction does not increase, since it does not depend on the electric field (Moruzzi et al., 1968).

3.1.4. Optical Signature Produced by Halos

Figure 8 shows the temporal evolution of the main emission spectral bands in the first 6 ms of halos produced by two different lightning discharges. In this plot, emissions of the first and second positive systems of molecular nitrogen, as well as the LBH band, have been obtained by summing the optical emission contribution from each vibrationally excited level. We analyze the optical emission from each species:

1. Emissions from excited states of molecular nitrogen: The first positive system of the molecular nitrogen dominates over other bands, followed by the second positive system of the same molecule. The intensity of the LBH band is comparable to the intensity of the second positive system. The number of emitted photons per second in the first negative system are around 3 orders of magnitude lower than optical emissions of the first positive system. It is interesting to note that the temporal position of each intensity peak is different as a consequence of the different lifetimes of each of the emitting species.

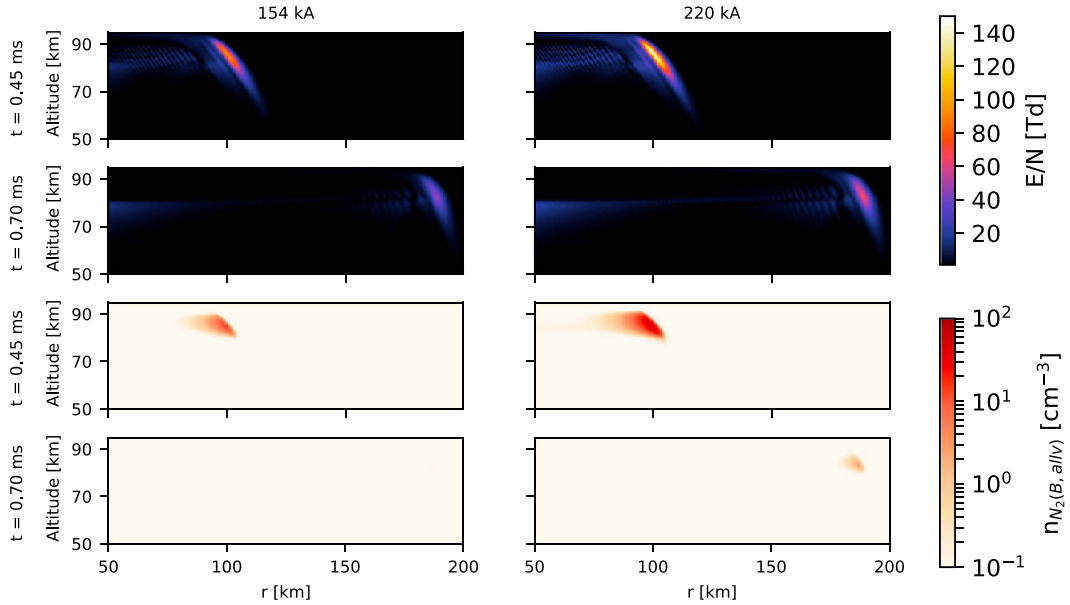

Figure 10. Reduced electric fields and densities of $N_2(B^3\Pi_g$, all v) in the upper atmosphere produced by two different vertical cloud-to-ground lightning discharges. The current peak values associated to each discharge are 154 and 220 kA). We show results 0.45 and 0.70 ms after the beginning of each discharge.

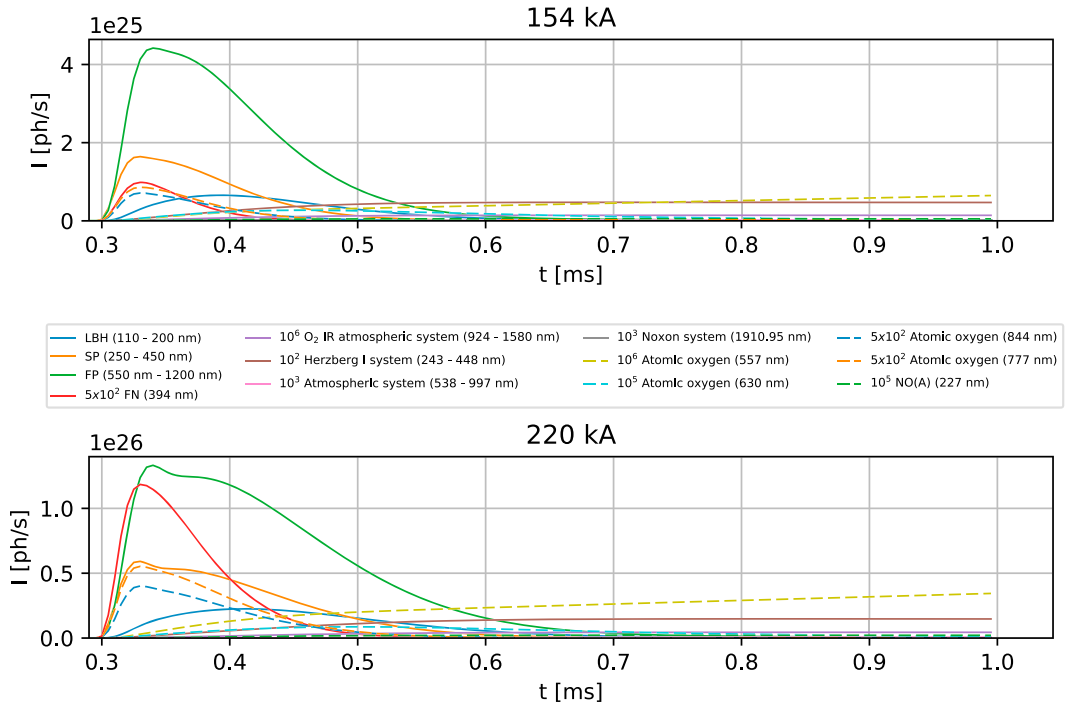

Figure 11. Temporal evolution of the total emitted photons per second (for the main spectral bands) from elves. This figure shows results for two elves triggered by two cloud-to-ground lightning discharges producing current peaks of 154 and 220 kA. As in Figure 8, some lines have been multiplied by different factors in an effort to plot all of them together. LBH, SP, FP, and FN correspond to the Lyman-Birge-Hopfield band and second positive, first positive, and first negative systems of the molecular nitrogen, respectively.

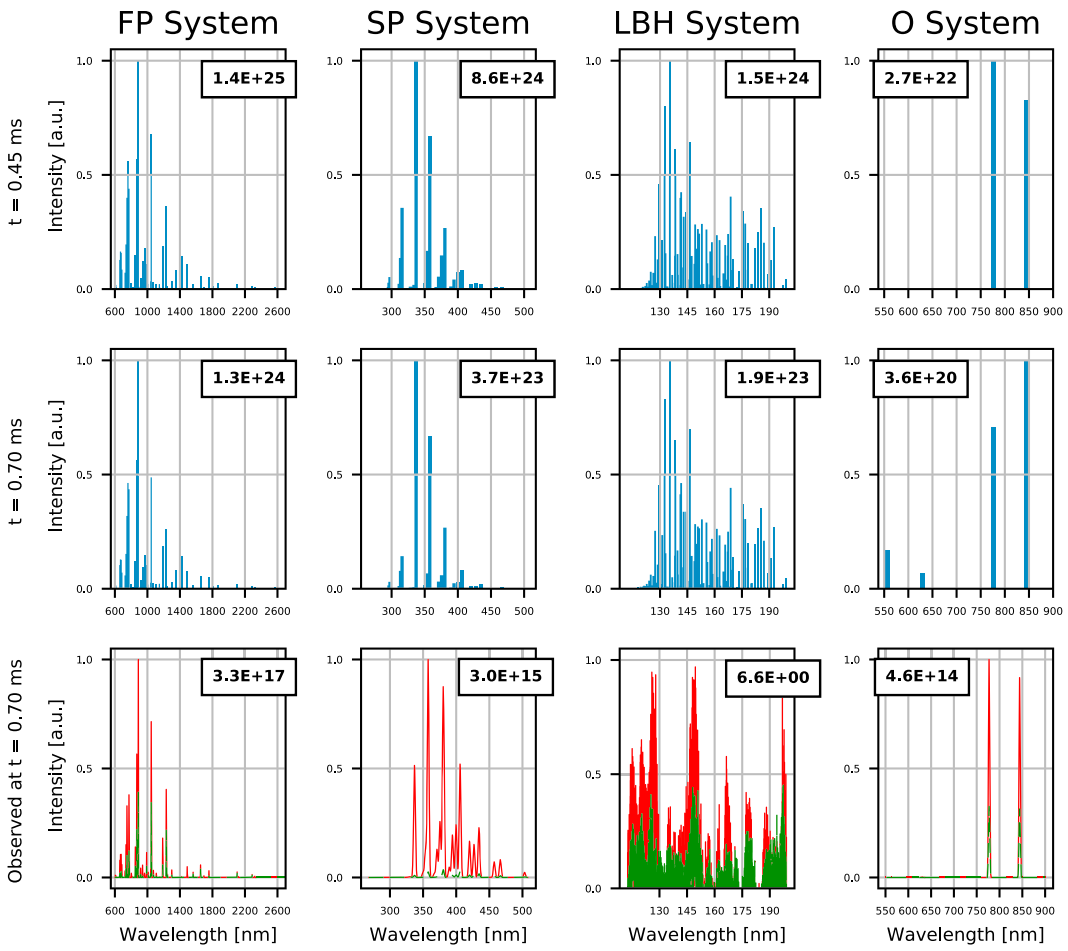

Figure 12. Calculated spectra of elves produced by a cloud-to-ground lightning discharge with a current peak of 220 kA for different bands. The first and the second rows show the emission spectra at the source, while the third row shows the predicted observed spectra 0.70 ms after the onset of the lightning discharge at 3 km (red solid line) and 275 m (green dashed line) over the sea and at a horizontal distance of 350 km. We plot the intensity of the bands in arbitrary units, normalizing each subplot to the stronger transition in each band. The numbers in boxes correspond to photons per second in the case of emisson spectra, and photons per second and squared meters in the case of the predicted observed spectra.

2. Emissions from excited states of molecular oxygen: We obtain emitted photons from molecular oxygen in the spectral bands detailed in Table 1. As can be seen in Figure 8, emissions from molecular oxygen are always between 1 and 6 orders of magnitude lower than emissions from the first positive system of molecular nitrogen.
3. Emissions from excited states of atomic oxygen and nitric oxide: Figure 8 also shows the temporal emissions produced by radiative decay of electronically excited states of atomic oxygen (O) and nitric oxide (NO). In particular, our calculations indicate that some weak emissions corresponding to 227, 557, 630, 777, and 844 nm would be produced by halos. However, these emissions would possibly be too weak to be detected by current instruments. The low background density of atomic oxygen and nitric oxide is the reason behind these weak optical emissions.

Knowledge of the concentration of each vibrational level in $N_2(B^3\Pi_g, v = 0,\dots,6)$, $N_2(C^3\Pi_u, v = 0,\dots,4)$, and $N_2(a^1\Pi_g, v = 0,\dots,15)$ allows us to build the VDF of these electronically excited species (Luque & Gordillo-Vázquez, 2011b). Therefore, we can also derive systhetic emission spectrum of halos with vibrational resolution in the mentioned bands. Figure 9 shows calculated spectra of halos corresponding to different spectral bands. Furthermore, we plot in this figure the predicted observed spectra at different observer altitudes (3 km and 275 m) and at a horizontal distance of 350 km from the halo. The software MODTRAN 5 (Berk et al., 2005) has been used to calculate the optical transmittance of the atmosphere needed to derive

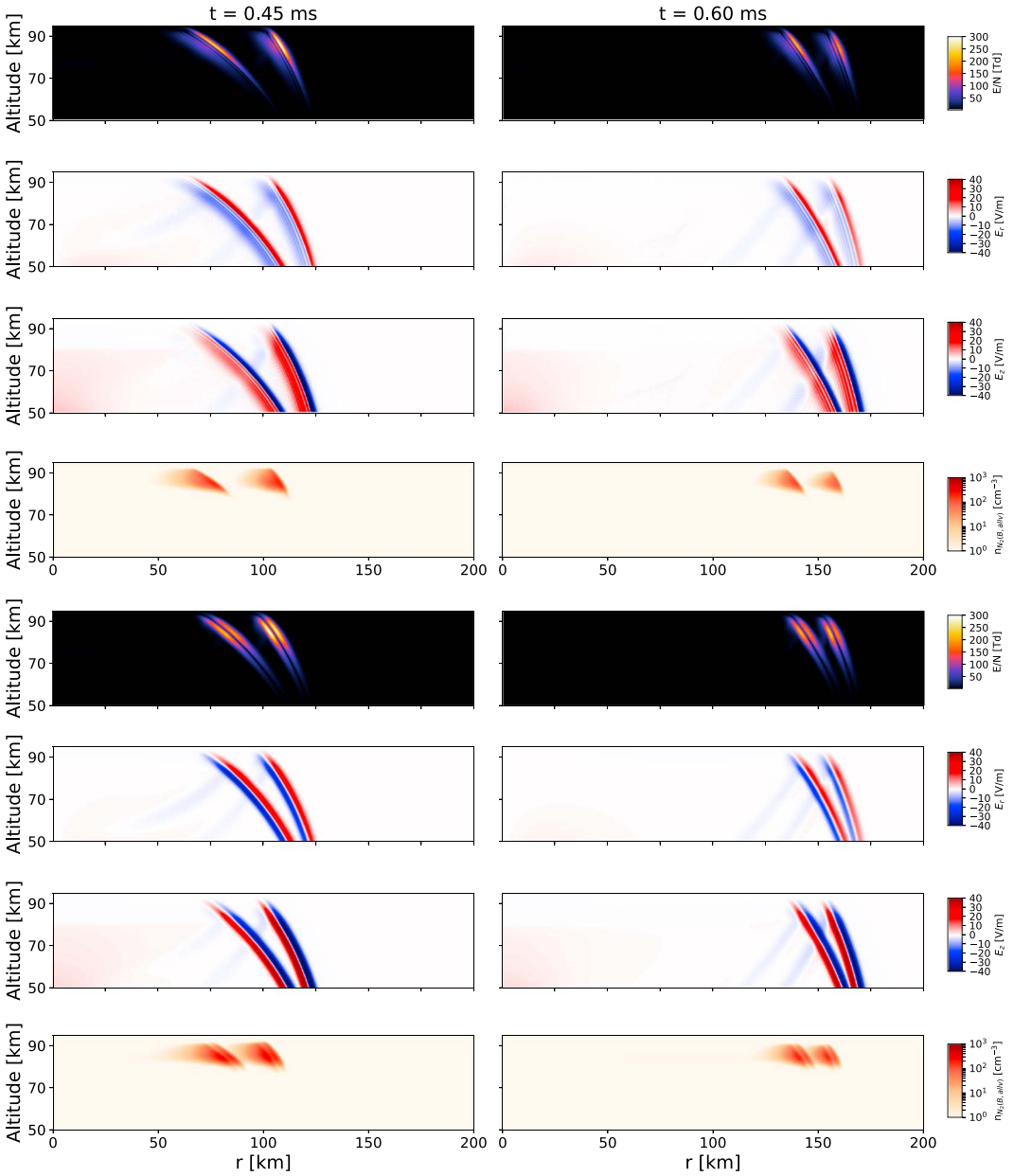

Figure 13. Reduced electric field, E_r and E_z electric field components and the density of $N_2(B^3\Pi_g$, all v) in the upper atmosphere produced by compact intracloud discharges and energetic in-cloud pulses. We show results corresponding to 0.45 and 0.60 ms after the beginning of the discharge.

the predicted observed spectra. In the case of a spacecraft observing from its orbit, the observed spectra would be similar to the emitted spectra at the source, given the low attenuation of light in the atmosphere at altitudes above 80 km of altitude.

Let us compare the obtained observed halo spectra with the ones previously calculated by Gordillo-Vázquez et al. (2011, 2012). It can be seen how the first and second positive systems, as well as the LBH systems of the molecular nitrogen are in good agreement with halo spectra shown in Gordillo-Vázquez et al. (2011, 2012).

3.2. FDTD Model Results

In this section we analyze elves triggered by CG lightning discharges, CIDs, and EIPs. We use the models described in section 2.3 to investigate the local chemical impact and optical signature produced by EMPs in the lower ionosphere.

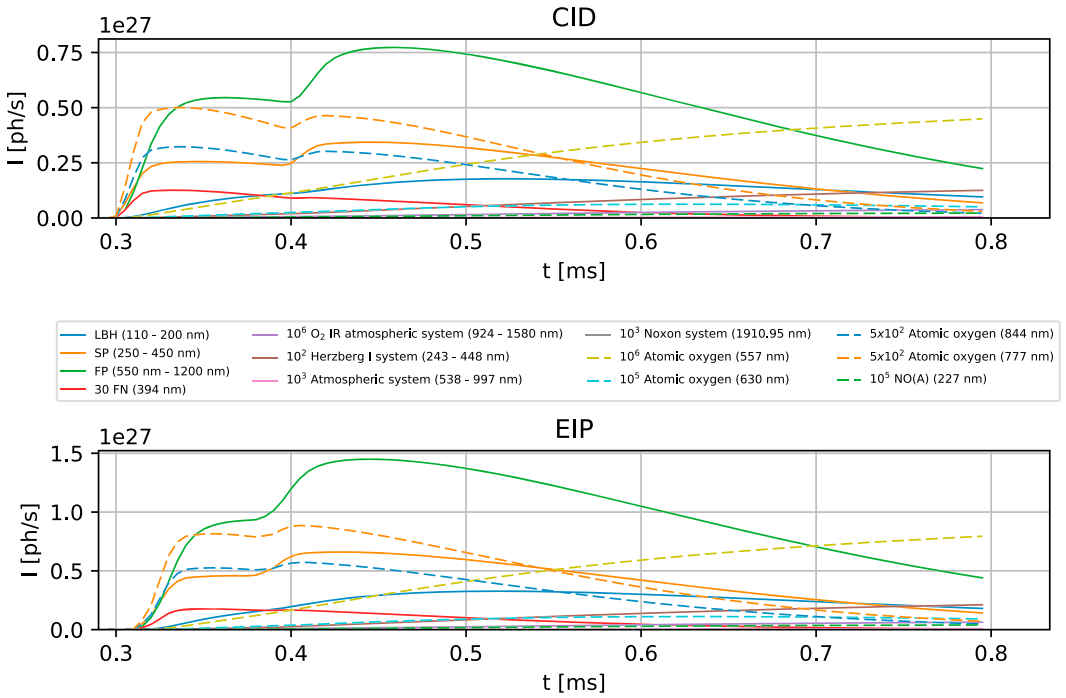

Figure 14. Temporal evolution of the total emitted photons per second (for the main spectral bands) from elves produced by compact intracloud discharges (CIDs) and energetic in-cloud pulses (EIPs). As in Figure 8, some lines have been multiplied by different factors in an effort to plot all of them together. LBH, SP, FP, and FN correspond to Lyman-Birge-Hopfield band and second positive, first positive, and first negative systems of molecular nitrogen, respectively.

3.2.1. Chemical Impact and Optical Signature Produced by CG Lightning-Generated Elves

Figure 10 shows the reduced electric fields and densities of the emitting species $N_2(B^3\Pi_g$, all $v)$ in the upper atmosphere produced by two different vertical CG lightning discharges. The pulse emitted by the temporal derivative of the current (19) and the quasi-electrostatic field produced by the charge accumulation can be distinguished. The shape of the elves can be clearly distinguished in the last two rows of Figure 10 at around 88 km of altitude, where the density of $N_2(B^3\Pi_g$, all $v)$ will produce toroidal-shaped optical emissions in the 337-nm spectral line by radiative decay. This figure also shows the quasi-electrostatic field produced by CG discharges in the first horizontal 50 km from the source, which would produce a halo.

In order to obtain the optical emissions produced by the elve itself without the influence of the halo, we calculate the part of the emissions produced from altitudes between 82 to 90 km and from radial distances between 50 and 200 km away from the source. The obtained temporal evolution of the main optical emissions triggered by the mentioned CG discharges are shown Figure 11. The FP system of N_2 dominates over the rest of emissions, reaching its maximum 0.42 ms after the beginning of the discharge. The ratio between each emitted band is similar to the case of halos, except in the case of the first negative system of the most powerful discharge, whose relative importance increases given the high reduced electric field.

We also compute the emission spectra of elves. Figure 12 shows the main spectral bands where the elve can be detected. The observed spectra at points located 275 m and 3 km above the sea level and at a horizontal distance of 350 km from the elve is also shown in the figure.

Let us now analyze the local chemical impact of elves by estimating the production of NO molecules. We analyze the elves triggered by CG lightning discharges whose current peaks are 90, 154, and 220 kA. The weakest of these discharges produces an elve slightly above the ISUAL detection threshold, estimated in parent lightning discharges with peak currents about 80 kA (Chern et al., 2014; Kuo et al., 2007), while the strongest discharge corresponds to a typical CG with a risetime of 40μs (Rakov & Uman, 2003). The simulated elves triggered by CG lightning discharges with current peaks of 90, 110, and 220 kA create about 5×10^{17}, 6×10^{19} NO, and 4×10^{20} NO molecules, respectively, in agreement with Blaes et al. (2016). We also compute (following the method described in section 3.1.3) the total amount of energy locally deposited in the mesosphere

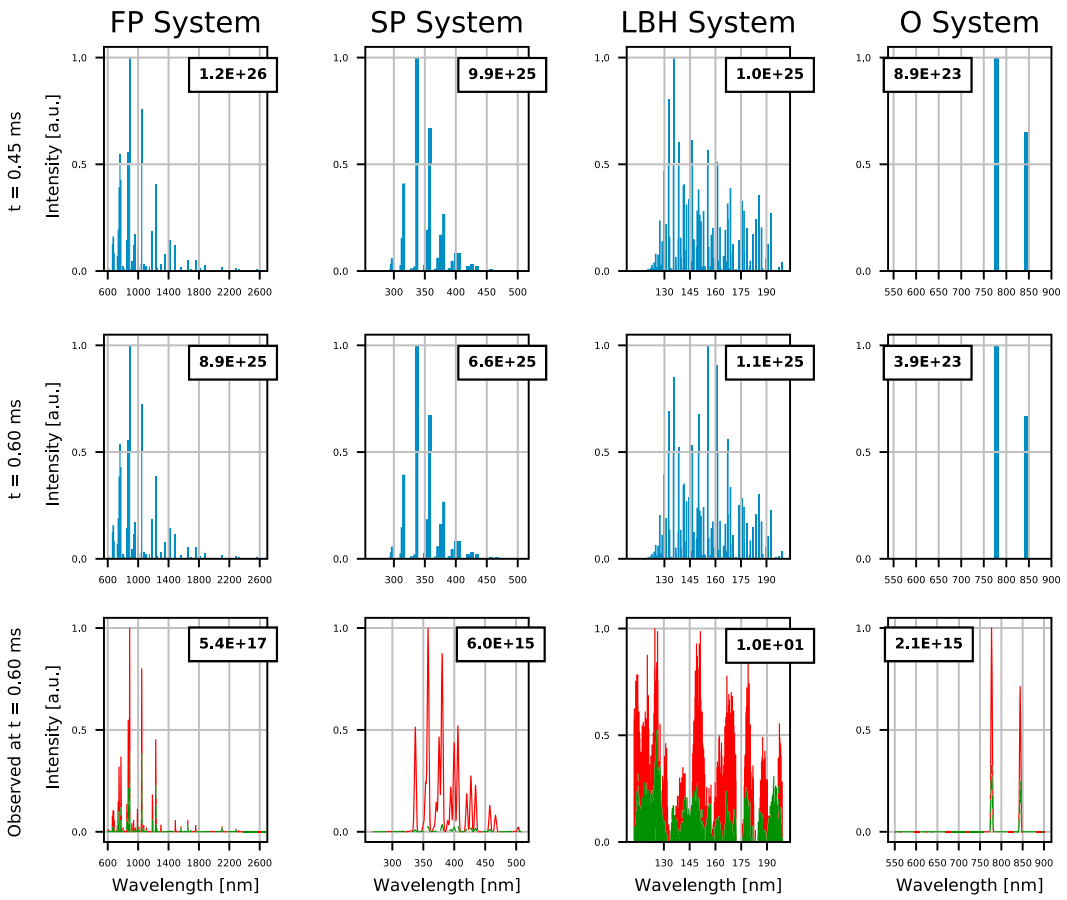

Figure 15. Calculated spectra of elves produced by a compact intracloud discharge. The first and the second rows show the emission spectra at the source, while the third row shows the observed spectra 0.6 ms after the onset of the compact intracloud discharge at 275 m (red solid line) and 3 km (green dashed line) over the sea and at a horizontal distance of 350 km. We plot the intensity of the bands in arbitrary units, normalizing each subplot to the stronger transition in each band. The numbers in boxes correspond to photons per second in the case of emission spectra, and photons per second and squared meters in the case of the predicted observed spectra. FP = first positive; SP = second positive; LBH = Lyman-Birge-Hopfield band.

by these three elves, obtaining 2×10^5, 7×10^5, and 10^6 J, respectively. According to these quantities, the production rate of NO by elves in terms of energy would be in the range between 2.5×10^{12} and 4×10^{14} molecules of NO/J, that is, between 4 and 2 orders of magnitude below the NO production rate of halos. According to ISUAL observations, the global annual occurrence of TLEs is about 1.2×10^7 (Chern et al., 2014), among which 74% are elves. The results of our elve simulations together with the observation of elves by ISUAL allow us to estimate that the total global amount of NO created by elves ranges between 10^{-10} and 10^{-7} Tg N/year. This quantity is between 10 and 7 orders of magnitude lower than the estimated global annual production of NO by lightning discharges (between 5 and 9 Tg N/year; Nault et al., 2017; Schumann & Huntrieser, 2007). The global chemical influence of elves is then negligible.

3.2.2. Chemical Impact and Optical Signature Produced by CID-Generated and EIP-Generated Elves

As explained in section 2.3, we investigate the local chemical impact and optical signature produced by CIDs and EIPs. The discharge current used as source is the one proposed by Watson and Marshall (2007) for the case of CIDs and by Liu et al. (2017) for the case of EIPs.

Figure 13 shows the reduced electric field and the density of $N_2(B^3\Pi_g$, all $v)$ produced by both a CID and an EIP. This figure also shows the electric field components E_r and E_z produced by the discharges. As discovered by Newsome and Inan (2010) and modeled by Marshall et al. (2015) and by Liu et al. (2017), the EMP produced by CIDs and EIPs trigger a succession of two elves or elve *doublet* as a consequence of the primary wave ground-reflexion. In addition, Figure 13 shows how each pulse is formed by two subpulses with different

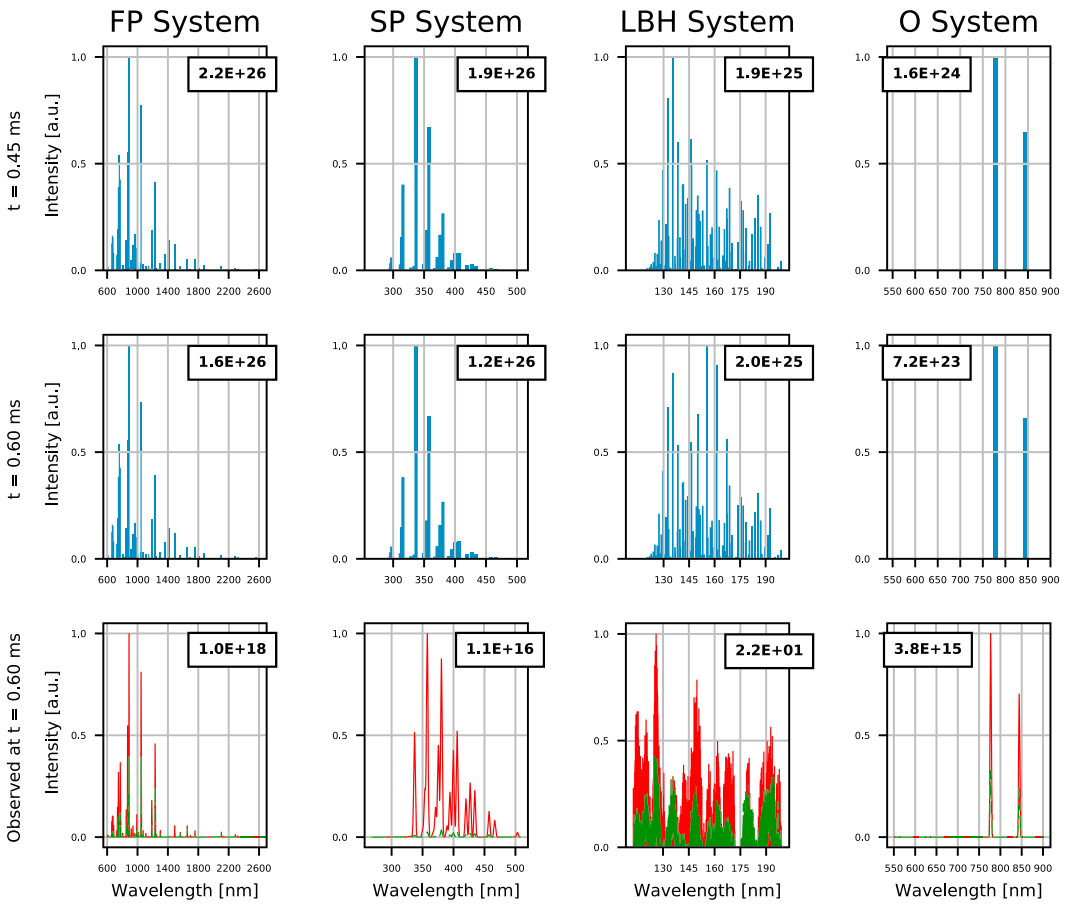

Figure 16. Calculated spectra of elves produced by an energetic in-cloud pulse. The first and the second rows show the emission spectra at the source, while the third row shows the observed spectra 0.6 ms after the onset of the energetic in-cloud pulse at 275 m (red solid line) and 3 km (green dashed line) over the sea and at a horizontal distance of 350 km. We plot the intensity of the bands in arbitrary units, normalizing each subplot to the stronger transition in each band. The numbers in boxes correspond to photons per second in the case of emission spectra, and photons per second and squared meters in the case of the predicted observed spectra.

polarization, due to the fast sign reversal of the derivative of the electric current at the source (Liu et al., 2017; Watson & Marshall, 2007). The delay between the consecutive elves at a given distance from the center is different in the case of CIDs and EIPs as a consequence of the different altitudes of the current sources. The total number of NO molecules produced by these simulated CID- and EIP-driven elves is about 10^{21}.

Figure 14 shows the obtained temporal evolution of the main optical emissions triggered by a CID and an EIP. As the current source temporal profile used in this work is different for the case of CIDs and EIPs (Liu et al., 2017; Watson & Marshall, 2007), the temporal dependence of the optical emissions due to each event differs. The altitude of each event influences the delay between the peaks of maximum emissions, as can be seen after comparing the relative maximum of the emissions plotted in each panel of Figure 14.

We plot in Figures 15 and 16 the main spectral bands where the CID- and the EIP-produced double elves emit photons. As in the last section, we predict the spectra as they would be observed at 275 m and 3 km above the sea level and at a horizontal distance of 350 km from the elve.

4. Comparison of Predicted Spectra

In this section we analyze and compare the predicted spectra of halos and elves (Figures 9, 12, 15, and 16). We also plot with more detail in Figure 17 the observed spectral bands corresponding to the FP and the SP systems of N_2 of each TLE, where we have added the spectra of a CG-driven elve produced by a lightning discharge with an extreme CMC of 1600 C m (276 kA).

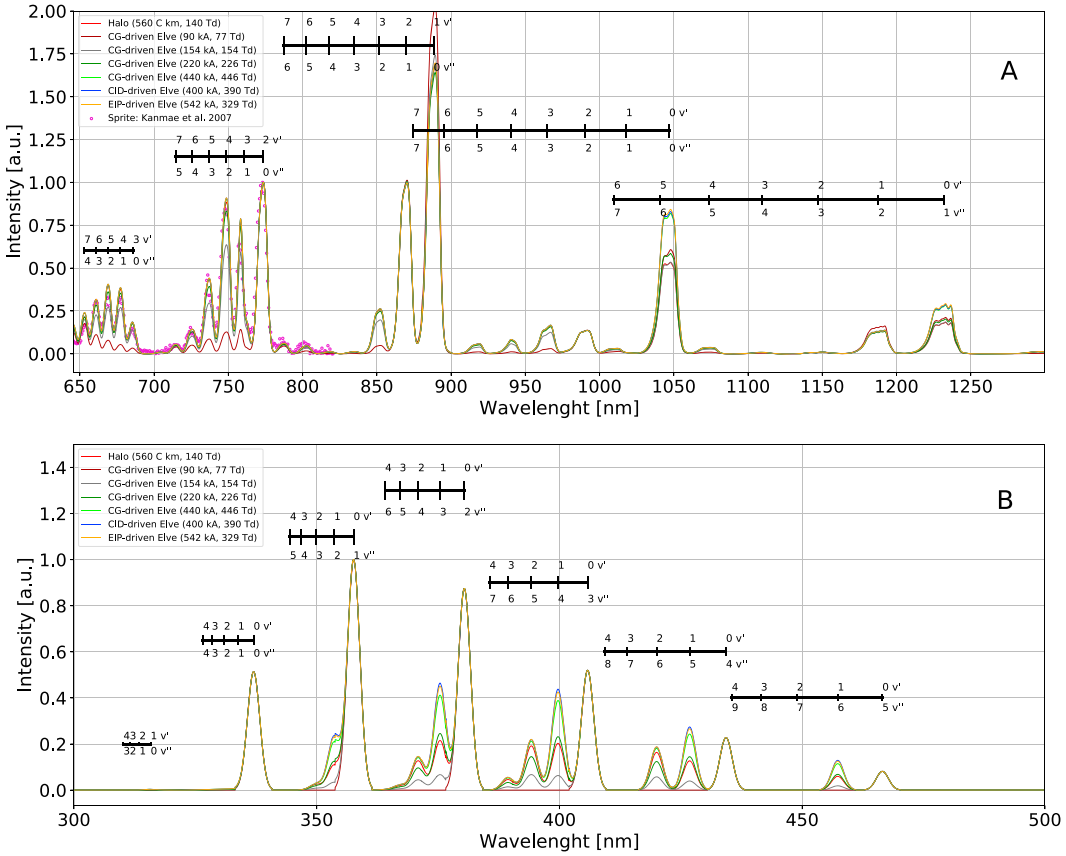

Figure 17. Calculated spectra of (a) the first positive system of N_2 and (b) the second positive system of N_2 for halos and elves produced by different discharges as seen by an observer located at an altitude of 3 km and a horizontal distance of 350 km. The magenta circles correspond to the sprite spectrum observed by Kanmae et al. (2007). The observation of this sprite was performed from an altitude of 3.25 km and at horizontal distance of 350 km, and the observed region of the sprite was between 84 and 86 km of altitude. The normalization of the spectra of the first positive and the second positive systems of N_2 spectra were done with respect to the (2,0) and the (0,1) transitions, respectively. We have selected the spectra at the moment of maximum emission of each TLE. The legend indicates the characteristics of the parent lightning and the maximum reduced electric field reached inside each TLE. CG = cloud-to-ground; CID = compact intracloud discharge; EIP = energetic in-cloud pulse; TLE = transient luminous event.

There are some slight differences between the spectra of halos, CG-driven elves, CID-driven elves, and EIP-driven elves plotted in Figures 9, 12, 15, and 16. These differences can be attributed to the influence of the reduced electric field in the ionosphere. This is shown in Figure 17, where the spectra of the CG-driven elves depend on the lightning CMC. Also, the spectra of the elves generated by the 1,600 C km CG discharge, the CID, and the EIP are similar.

Observed spectra of halos are very noisy as a consequence of their low luminosity, as the one recorded shown in Wescott et al. (2001) and later on analyzed by Gordillo-Vázquez et al. (2011). However, we can compare our results with the optical sprite spectrum observed by Kanmae et al. (2007). The sprite region observed by Kanmae et al. (2007) was located at an altitude between 84 and 86 km, while the observation point was located at a mountain with an altitude of about 3 km and at a horizontal distance of 350 km from the TLE. Figure 17 shows a comparison between the predicted spectra for the first and second positive systems of N_2 of halos and elves together with the sprite spectrum observed by Kanmae et al. (2007). It can be seen that the predicted spectra of the FP system of N_2 agrees with reported observations.

5. Conclusions

Tropospheric electrical discharges such as CG lightning, CIDs, and EIPs can produce mesospheric optical emissions known as TLEs. The electromagnetic fields that produce TLEs can also trigger a cascade of chemical reactions producing a local chemical impact in the mesosphere. The main aim of this work has been

to contribute to the knowledge of the characteristics of halos and elves, some of the most frequent TLEs, as well as to quantify their chemical signature. To achieve our goal, we have developed two different self-consistent models based on previous works (Inan et al., 1991; Pasko et al., 1995) to study TLEs triggered by a single lightning discharge. Both models calculate the temporal evolution of more than 130 species in the lower ionosphere interacting through over 1,000 chemical reactions, some of which are triggered by the lightning-produced electric field in the upper mesosphere and lower ionosphere. We have calculated the vibrational distribution of some electronically excited states of N_2 to obtain a detailed description of the FP and SP systems of the N_2 and the N_2 LBH bands to calculate synthetic spectra. In addition, we have considered the rotational structure of the FP system of N_2 and its corresponding spectrum. Finally, we have computed the effect of air absorption in the emitted optical emissions, predicting the observed spectra of the simulated TLEs at different distances from the source. This approach has enabled us to compare the characteristics of halos and elves produced by different tropospheric discharges.

The first developed model has allowed us to predict the spectra of a single halo and its chemical impact in the mesosphere after 1 s of being triggered. To perform this long-time simulation of a single halo, we have avoided the sprite inception problem simulating a second discharge that removes the electric field produced by the first one several milliseconds later. The calculated spectra agree with previous model results (Gordillo-Vázquez et al., 2011, 2012) and with the spectra of the FP system of N_2 of sprites detected by Kanmae et al. (2007) and more recently with the high-resolution sprite spectra reported by Gordillo-Vázquez et al. (2018). In addition, our models predict a nonnegligible enhancement of local mesospheric N_2O, NO, and metastable species as a consequence of this glow discharge. Future observations are needed to confirm the local chemical impact of halos and to establish their possible regional or global influence in the mesosphere. We estimate a global production of NO due to halos and elves of the order of 10^{-7} Tg N/year, which is not significant for global scale chemistry.

We have developed another model to simulate elves produced by CG lightning discharges, CIDs, and EIPs. We have estimated for the first time the optical spectra of elves triggered by CIDs and EIPs. According to our results, it is not the type of discharge that influences the observed spectra of the produced TLEs but the value of the reduced electric field reached in the lower ionosphere. Despite the similarities in the spectra of elves produced by CG lightning discharges and CIDs or EIPs, the appearance of the elves produced by each type of discharge would be different. The former would usually be detected as single elves, while the latter would appear as double elves, as previously investigated by Marshall et al. (2015) and Liu et al. (2017).

Acknowledgments
This work was supported by the Spanish Ministry of Science and Innovation, MINECO, under projects ESP2015-69909-C5-2-R and ESP2017-86263-C4-4-R and by the EU through the H2020 Science and Innovation with Thunderstorms (SAINT) project (Ref. 722337) and the FEDER program. F. J. P. I. acknowledges a PhD research contract, code BES-2014-069567. A. L. was supported by the European Research Council (ERC) under the European Union's H2020 program/ERC grant agreement 681257. The simulation data and plot codes presented here are available from figshare repository at https://figshare.com/s/f1c9f6c7bc728d6669dd. Alternatively, requests for the data and codes used to generate or displayed in figures, graphs, plots, or tables are also available after a request is made to the authors F. J. P. I. (fjpi@iaa.es), A. L. (aluque@iaa.es), or F. J. G. V. (vazquez@iaa.es).

References

Adachi, T., Sato, M., Ushio, T., Yamazaki, A., Suzuki, M., Kikuchi, M., et al. (2016). Identifying the occurrence of lightning and transient luminous events by nadir spectrophotometric observation. *Journal of Atmospheric and Solar-Terrestrial Physics*, *145*, 85–97. https://doi.org/10.1016/j.jastp.2016.04.010

Albritton, D. (1978). Ion-neutral reaction-rate constants measured in flow reactors through 1977. *Atomic Data and Nuclear Data Tables*, *22*(1), 1–89.

Arnone, E., Kero, A., Dinelli, B. M., Enell, C.-F., Arnold, N. F., Papandrea, E., et al. (2008). Seeking sprite-induced signatures in remotely sensed middle atmosphere NO_2. *Geophysical Research Letters*, *35*, L05807. https://doi.org/10.1029/2007GL031791

Barrington-Leigh, C. P., & Inan, U. S. (1999). Elves triggered by positive and negative lightning discharges. *Geophysical Research Letters*, *26*, 683–686. https://doi.org/10.1029/1999GL900059

Barrington-Leigh, C. P., Inan, U. S., & Stanley, M. (2001). Identification of sprites and elves with intensified video and broadband array photometry. *Journal of Geophysical Research*, *106*, 1741–1750. https://doi.org/10.1029/2000JA000073

Bates, D. (1988). Transition probabilities of the bands of the oxygen systems of the nightglow. *Planetary and Space Science*, *36*(9), 869–873. https://doi.org/10.1016/0032-0633(88)90092-X

Bering, E. A., Benbrook, J. R., Bhusal, L., Garrett, J. A., Paredes, A. M., Wescott, E. M., et al. (2004). Observations of transient luminous events (TLEs) associated with negative cloud to ground (-CG) lightning strokes. *Geophysical Research Letters*, *31*, L05104. https://doi.org/10.1029/2003GL018659

Bering, E. A., Benbrook, J. R., Garrett, J. A., Paredes, A. M., Wescott, E. M., Moudry, D. R., et al. (2002). Sprite and elve electrodynamics. *Advances in Space Research*, *30*, 2585–2595. https://doi.org/10.1016/S0273-1177(02)80350-7

Bering, E. A., Bhusal, L., Benbrook, J. R., Garrett, J. A., Jackson, A. P., Wescott, E. M., et al. (2004). The results from the 1999 sprites balloon campaign. *Advances in Space Research*, *34*, 1782–1791. https://doi.org/10.1016/j.asr.2003.05.043

Berk, A., Anderson, G. P., Acharya, P. K., Bernstein, L. S., Muratov, L., Lee, J., et al. (2005). MODTRAN 5: A reformulated atmospheric band model with auxiliary species and practical multiple scattering options: Update, *Algorithms and technologies for multispectral, hyperspectral, and ultraspectral imagery XI* (Vol. 5806, pp. 662–668). Orlando, FL: International Society for Optics and Photonics.

Biondi, M., Bortner, M., & Bauer, T. (1971). Defense nuclear agency reaction rate handbook. DNA 1948H (US GPO, Washington, DC, 1972).

Blaes, P. R., Marshall, R. A., & Inan, U. S. (2016). Global occurrence rate of elves and ionospheric heating due to cloud-to-ground lightning. *Journal of Geophysical Research: Space Physics*, *121*, 699–712. https://doi.org/10.1002/2015JA021916

Blanc, E., Lefeuvre, F., Roussel-Dupré, R., & Sauvaud, J. A. (2007). A microsatellite project dedicated to the study of impulsive transfers of energy between the Earth atmosphere, the ionosphere, and the magnetosphere. *Advances in Space Research*, *40*, 1268–1275. https://doi.org/10.1016/j.asr.2007.06.037

Boeck, W. L., Vaughan, O. H., Blakeslee, R. J., Vonnegut, B., & Brook, M. (1992). Lightning induced brightening in the airglow layer. *Geophysical Research Letters*, *19*(2), 99–102.

Borst, W. L., & Zipf, E. C. (1970). Cross section for electron-impact excitation of the (0,0) first negative band of N_2^+ from threshold to 3 keV. *Physical Review A*, *1*, 834. https://doi.org/10.1103/PhysRevA.1.834

Brasseur, G. P., & Solomon, S. (1986). *Aeronomy of the middle atmosphere Edited by* 2nd. ed.Boston, Mass: Reidel.

Briggs, M. S., Fishman, G. J., Connaughton, V., Bhat, P. N., Paciesas, W. S., Preece, R. D., et al. (2010). First results on terrestrial gamma ray flashes from the Fermi Gamma-ray Burst Monitor. *Journal of Geophysical Research*, *115*, A07323. https://doi.org/10.1029/2009JA015242

Cacciatore, M., Kurnosov, A., & Napartovich, A. (2005). Vibrational energy transfer in N2–N2 collisions: A new semiclassical study. *The Journal of Chemical Physics*, *123*(17), 174315. https://doi.org/10.1063/1.2101445

Calo, J. M., Axtmann, R. C., & Crowder, L. (1971). Collisional deactivation of CO_2 and CO luminescence. *Journal of Chemical Physics*, *55*, 5847–5847. https://doi.org/10.1063/1.1675774

Capitelli, M., Ferreira, C. M., Gordiets, B. F., & Osipov, A. I. (2000). *Plasma kinetics in atmospheric gases, atomic, optical and plasma physics*. Berlin, Germany: Springer.

Cartwright, D. C., Trajmar, S., Chutjian, A., & Williams, W. (1977). Electron impact excitation of the electronic states of N_2. II. Integral cross sections at incident energies from 10 to 50 eV. *Physical Review A*, *16*, 1041–1051. https://doi.org/10.1103/PhysRevA.16.1041

Castillo, M., Herrero, V. J., Méndez, I., & Tanarro, I. (2004). Spectrometric and kinetic study of a modulated glow air discharge. *Plasma Sources Science and Technology*, *13*, 343–350.

Chang, S. C., Kuo, C. L., Lee, L. J., Chen, A. B., Su, H. T., Hsu, R. R., et al. (2010). ISUAL far-ultraviolet events, elves, and lightning current. *Journal of Geophysical Research*, *115*, A00E46. https://doi.org/10.1029/2009JA014861

Chapman, S., & Cowling, T. G. (1970). *The mathematical theory of non-uniform gases: An account of the kinetic theory of viscosity, thermal conduction and diffusion in gases*. Cambridge: Cambridge University Press.

Chern, J. L., Wu, A. M., & Lin, S. F. (2014). Globalization extension of transient luminous events from FORMOSAT-2 observation. *Acta Astronautica*, *98*, 64–70. https://doi.org/10.1016/j.actaastro.2014.01.014

Christian, H. J., Blakeslee, R. J., Boccippio, D. J., Boeck, W. L., Buechler, D. E., Driscoll, K. T., et al. (2003). Global frequency and distribution of lightning as observed from space by the Optical Transient Detector. *Journal of Geophysical Research*, *108*(D10), 4005. https://doi.org/10.1029/2002JD002347

Cummer, S. A., Briggs, M. S., Dwyer, J. R., Xiong, S., Connaughton, V., Fishman, G. J., et al. (2014). The source altitude, electric current, and intrinsic brightness of terrestrial gamma ray flashes. *Geophysical Research Letters*, *41*, 8586–8593. https://doi.org/10.1002/2014GL062196

Cummer, S. A., & Lyons, W. A. (2004). Lightning charge moment changes in U.S. High Plains thunderstorms. *Geophysical Research Letters*, *31*, L05114. https://doi.org/10.1029/2003GL019043

Dagdigian, P. J., Forch, B. E., & Miziolek, W. (1988). Collisional transfer between and quenching of the 3p 3P and 5P states of the oxygen atom. *Chemical Physics Letters*, *148*, 299–308. https://doi.org/10.1016/0009-2614(88)87276-2

Dormand, J. R., & Prince, P. J. (1980). A family of embedded Runge-Kutta formulae. *Journal of Computational and Applied Mathematics*, *6*, 19–26. https://doi.org/10.1016/0771-050X(80)90013-3

Erdman, P. W., & Zipf, E. C. (1987). Excitation of the OI (3s 5S0-3p 5P; 7774 Å) multiplet by electron impact on CO_2. *Journal Chemical Physics*, *87*, 4540–4545. https://doi.org/10.1063/1.453696

Fahr, H., & Müller, K. G. (1967). Ionenbewegung unter dem Einfluß von Umladungsstößen. *Zeitschrift für Physik A Hadrons and Nuclei*, *200*(4), 343–365.

Franz, R. C., Nemzek, R. J., & Winckler, J. R. (1990). Television image of a large upward electrical discharge above a thunderstorm system. *Science*, *249*, 48–51. https://doi.org/10.1126/science.249.4964.48

Frey, H. U., Mende, S. B., Cummer, S. A., Li, J., Adachi, T., Fukunishi, H., et al. (2007). Halos generated by negative cloud-to-ground lightning. *Geophysical Research Letters*, *34*, L18801. https://doi.org/10.1029/2007GL030908

Fukunishi, H., Takahashi, Y., Kubota, M., Sakanoi, K., Inan, U. S., & Lyons, W. A. (1996). Elves: Lightning-induced transient luminous events in the lower ionosphere. *Geophysical Research Letters*, *23*, 2157–2160. https://doi.org/10.1029/96GL01979

Gilmore, F. R., Laher, R. R., & Espy, P. J. (1992). Franck-Condon factors, r-centroids, electronic transition moments, and Einstein coefficients for many nitrogen and oxygen band systems. *Journal of Physical and Chemical Reference Data*, *21*, 1005. https://doi.org/10.1063/1.555910

Gordiets, B. F., Ferreira, C. M., Guerra, V. L., Loureiro, J. M. A. H., Nahorny, J., Pagnon, D., et al. (1995). Kinetic model of a low-pressure $N_2/-O_2$ flowing glow discharge. *IEEE Transactions on Plasma Science*, *23*, 750–768. https://doi.org/10.1109/27.467998

Gordillo-Vázquez, F. J. (2008). Air plasma kinetics under the influence of sprites. *Journal of Physics D: Applied Physics*, *41*(23), 234016. https://doi.org/10.1088/0022-3727/41/23/234016

Gordillo-Vázquez, F. J. (2010). Vibrational kinetics of air plasmas induced by sprites. *Journal of Geophysical Research*, *115*, A00E25. https://doi.org/10.1029/2009JA014688

Gordillo-Vázquez, F. J., Luque, A., & Simek, M. (2011). Spectrum of sprite halos. *Journal of Geophysical Research*, *116*, A09319. https://doi.org/10.1029/2011JA016652

Gordillo-Vázquez, F. J., Luque, A., & Simek, M. (2012). Near infrared and ultraviolet spectra of TLEs. *Journal of Geophysical Research*, *117*, A05329. https://doi.org/10.1029/2012JA017516

Gordillo-Vázquez, F. J., Passas, M., Luque, A., Sánchez, J., Velde, O. A., & Montanyá, J. (2018). High spectral resolution spectroscopy of sprites: A natural probe of the mesosphere. *Journal of Geophysical Research: Atmospheres*, *123*, 2336–2346. https://doi.org/10.1002/2017JD028126

Gudmundsson, J. T., Kouznetsov, I. G., Patel, K. K., & Lieberman, M. A. (2001). Electronegativity of low-pressure high-density oxygen discharges. *Journal of Physics D: Applied Physics*, *34*, 1100.

Guerra, V., & Loureiro, J. (1999). Kinetic model of a low-pressure microwave discharge in O_2-H_2 including the effects of O^- ions on the characteristics for plasma maintenance. *Plasma Sources Science and Technology*, *8*, 110. https://doi.org/10.1088/0963-0252/8/1/014

Gurevich, A. V., Medvedev, Y. V., & Zybin, K. P. (2004). New type discharge generated in thunderclouds by joint action of runaway breakdown and extensive atmospheric shower. *Physics Letters A*, *329*, 348–361. https://doi.org/10.1016/j.physleta.2004.06.099

Gurevich, A. V., & Zybin, K. P. (2001). Runaway breakdown and electric discharges in thunderstorms. *Physics Uspekhi*, *44*, 1119. https://doi.org/10.1070/PU2001v044n11ABEH000939

Hagelaar, G. J. M., & Pitchford, L. C. (2005). Solving the Boltzmann equation to obtain electron transport coefficients and rate coefficients for fluid models. *Plasma Sources Science and Technology*, *14*, 722–733. https://doi.org/10.1088/0963-0252/14/4/011

Heidler, F., Cvetic, J., & Stanic, B. (1999). Calculation of lightning current parameters. *IEEE Transactions on Power Delivery*, *14*(2), 399–404.

Herron, J. T., & Green, D. S. (2001). Chemical kinetics database and predictive schemes for nonthermal humid air plasma chemistry. Part II. Neutral species reactions. *Plasma Chemistry and Plasma Processing*, *21*(3), 459–481. https://doi.org/10.1023/A:1011082611822

Hu, W., Cummer, S. A., & Lyons, W. A. (2007). Testing sprite initiation theory using lightning measurements and modeled electromagnetic fields. *Journal of Geophysical Research*, *112*, D13115. https://doi.org/10.1029/2006JD007939

Inan, U. S., Barrington-Leigh, C., Hansen, S., Glukhov, V. S., Bell, T. F., & Rairden, R. (1997). Rapid lateral expansion of optical luminosity in lightning-induced ionospheric flashes referred to as "elves". *Geophysical Research Letters*, *24*, 583–586. https://doi.org/10.1029/97GL00404

Inan, U. S., Bell, T. F., & Rodriguez, J. V. (1991). Heating and ionization of the lower ionosphere by lightning. *Geophysical Research Letters*, *18*, 705–708. https://doi.org/10.1029/91GL00364

Inan, U., & Marshall, R. A. (2011). *Numerical electromagnetics: The FDTD method*. New York: Cambridge University Press.

Kabirzadeh, R., Lehtinen, N. G., & Inan, U. S. (2015). Latitudinal dependence of static mesospheric *E* fields above thunderstorms. *Geophysical Research Letters*, *42*, 4208–4215. https://doi.org/10.1002/2015GL064042

Kabirzadeh, R., Marshall, R. A., & Inan, U. S. (2017). Early/fast VLF events produced by the quiescent heating of the lower ionosphere by thunderstorms. *Journal of Geophysical Research: Atmospheres*, *122*, 6217–6230. https://doi.org/10.1002/2017JD026528

Kam, A. W., & Pipkin, F. M. (1991). Measurement of the lifetime of the metastable a'' $^1\Sigma_g^+$ state of N_2. *Physical Review A*, *43*, 3279–3284. https://doi.org/10.1103/PhysRevA.43.3279

Kamaratos, E. (2006). Active nitrogen and oxygen: Enhanced emissions and chemical reactions. *Chemical physics*, *323*, 271–294. https://doi.org/10.1016/j.chemphys.2005.09.026

Kanmae, T., Stenbaek-Nielsen, H. C., & McHarg, M. G. (2007). Altitude resolved sprite spectra with 3 ms temporal resolution. *Geophysical Research Letters*, *34*, L07810. https://doi.org/10.1029/2006GL028608

Karunarathne, S., Marshall, T. C., Stolzenburg, M., & Karunarathna, N. (2016). Electrostatic field changes and durations of narrow bipolar events. *Journal of Geophysical Research: Atmospheres*, *121*, 10,161–10,174. https://doi.org/10.1002/2016JD024789

Kazil, J., Kopp, E., Chabrillat, S., & Bishop, J. (2003). The University of Bern Atmospheric Ion Model: Time-dependent modeling of the ions in the mesosphere and lower thermosphere. *Journal of Geophysical Research*, *108*(D14), 4432. https://doi.org/10.1029/2002JD003024

Kossyi, I. A., Kostinsky, A. Y., Matveyev, A. A., & Silakov, V. P. (1992). Kinetic scheme of the non-equilibrium discharge in nitrogen-oxygen mixtures. *Plasma Sources Science and Technology*, *1*, 207–220. https://doi.org/10.1088/0963-0252/1/3/011

Kovacs, I. (1969). *Rotational structure in the spectra of diatomic molecules*. New York, USA: American Elsevier.

Krupenie, P. H. (1972). The spectrum of molecular oxygen. *Journal of Physical and Chemical Reference Data*, *1*(2), 423–534. https://doi.org/10.1063/1.3253101

Kuo, C.-L., et al. (2007). Modeling elves observed by FORMOSAT-2 satellite. *Journal of Geophysical Research*, *112*, A11312. https://doi.org/10.1029/2007JA012407

Kuo, C.-L., et al. (2013). Ionization emissions associated with N_2^+ 1N band in halos without visible sprite streamers. *Journal of Geophysical Research*, *118*, 5317–5326. https://doi.org/10.1002/jgra.50470

Kurnosov, A., Napartovich, A., Shnyrev, S., & Cacciatore, M. (2007). Vibrational energy exchanges in nitrogen: Application of new rate constants for kinetic modeling. *The Journal of Physical Chemistry A*, *30*, 7057–7065. https://doi.org/10.1021/jp071657a

Laher, R. R., & Gilmore, F. R. (1990). Updated excitation and ionization cross sections for electron impact on atomic oxygen. *Journal of Physical and Chemical Reference Data*, *19*, 277.

Lawton, S. A., & Phelps, A. V. (1978). Excitation of the $b^1\Sigma_g^+$ state of O_2 by low energy electrons. *The Journal of Chemical Physics*, *69*, 1055–1068. https://doi.org/10.1063/1.436700

Le Vine, D. M. (1980). Sources of the strongest RF radiation from lightning. *Journal of Geophysical Research*, *85*, 4091–4095. https://doi.org/10.1029/JC085iC07p04091

Lee, J. H., & Kalluri, D. K. (1999). Three-dimensional FDTD simulation of electromagnetic wave transformation in a dynamic inhomogeneous magnetized plasma. *IEEE Transactions on Antennas and Propagation*, *47*, 1146–1151. https://doi.org/10.1109/8.785745

Lepoutre, F., Louis, G., & Manceau, H. (1977). Collisional relaxation in CO_2 between 180 K and 400 K measured by the spectrophone method. *Chemical Physics Letters*, *48*, 509–514. https://doi.org/10.1016/0009-2614(77)85082-3

Linstrom, P., & Mallard, W. (2015). NIST chemistry webbook, NIST standard reference database 69. National Institute of Standards and Technology.

Liu, N. Y., Dwyer, J. R., & Cummer, S. A. (2017). Elves accompanying terrestrial gamma ray flashes. *Journal of Geophysical Research: Space Physics*, *122*, 10,563–10,576. https://doi.org/10.1002/2017JA024344

Liu, N., Dwyer, J. R., Stenbaek-Nielsen, H. C., & McHarg, M. G. (2015). Sprite streamer initiation from natural mesospheric structures. *Nature Communications*, *6*, 7540. https://doi.org/10.1038/ncomms8540

Lu, G., et al. (2010). Lightning mapping observation of a terrestrial gamma-ray flash. *Geophysical Research Letters*, *37*, L11806. https://doi.org/10.1029/2010GL043494

Luque, A. Computer code QTPlaskin (2011). Retrieved from https://github.com/aluque/qtplaskin

Luque, A., Dubrovin, D., Gordillo-Vázquez, F. J., Ebert, U., Parra-Rojas, F. C., Yair, Y., & Price, C. (2014). Coupling between atmospheric layers in gaseous giant planets due to lightning-generated electromagnetic pulses. *Journal of Geophysical Research: Space Physics*, *119*, 8705–8720. https://doi.org/10.1002/2014JA020457

Luque, A., & Ebert, U. (2009). Emergence of sprite streamers from screening-ionization waves in the lower ionosphere. *Nature Geoscience*, *2*, 757–760. https://doi.org/10.1038/ngeo662

Luque, A., & Gordillo-Vázquez, F. J. (2011a). Mesospheric electric breakdown and delayed sprite ignition caused by electron detachment. *Nature Geoscience*, *5*, 22–25. https://doi.org/10.1038/ngeo1314

Luque, A., & Gordillo-Vázquez, F. J. (2011b). Modeling and analysis of $N_2(B^3\Pi_g)$ and $N_2(C^3\Pi_u)$ vibrational distributions in sprites. *Journal of Geophysical Research*, *116*, A02306. https://doi.org/10.1029/2010JA015952

Lyu, F., Cummer, S. A., & McTague, L. (2015). Insights into high peak current in-cloud lightning events during thunderstorms. *Geophysical Research Letters*, *42*, 6836–6843. https://doi.org/10.1002/2015GL065047

Maggio, C. R., Marshall, T. C., & Stolzenburg, M. (2009). Estimations of charge transferred and energy released by lightning flashes. *Journal of Geophysical Research*, *114*, D14203. https://doi.org/10.1029/2008JD011506

Makhlouf, U. B., Picard, R. H., & Winick, J. R. (1995). Photochemical-dynamical modeling of the measured response of airglow to gravity waves: 1. Basic model for OH airglow. *Journal of Geophysical Research*, *100*(D6), 11289–11311. https://doi.org/10.1029/94JD03327

Marsh, D. R., Mills, M. J., Kinnison, D. E., Lamarque, J. F., Calvo, N., & Polvani, L. M. (2013). Climate change from 1850 to 2005 simulated in CESM1 (WACCM). *Journal of Climate*, *26*(19), 7372–7391. https://doi.org/10.1175/JCLI-D-12-00558.1

Marshall, R. A. (2012). An improved model of the lightning electromagnetic field interaction with the D-region ionosphere. *Journal of Geophysical Research*, *117*, A03316. https://doi.org/10.1029/2011JA017408

Marshall, R. (2014). Effect of self-absorption on attenuation of lightning and transmitter signals in the lower ionosphere. *Journal of Geophysical Research: Space Physics*, *119*, 4062–4076. https://doi.org/10.1002/2014JA019921

Marshall, R. A., da Silva, C. L., & Pasko, V. P. (2015). Elve doublets and compact intracloud discharges. *Geophysical Research Letters*, *42*, 6112–6119. https://doi.org/10.1002/2015GL064862

Marshall, R. A., & Inan, U. S. (2008). Elves and associated ionospheric density perturbations due to horizontal in-cloud lightning EMP. *American Geophysical Union, Fall Meeting 2008, abstract id. AE13A-0300*.

Marshall, R. A., Inan, U. S., & Glukhov, V. S. (2010). Elves and associated electron density changes due to cloud-to-ground and in-cloud lightning discharges. *Journal of Geophysical Research*, *115*, A00E17. https://doi.org/10.1029/2009JA014469

Marshall, R. A., Inan, U. S., & Lyons, W. A. (2006). On the association of early/fast very low frequency perturbations with sprites and rare examples of VLF backscatter. *Journal of Geophysical Research*, *111*, D19108. https://doi.org/10.1029/2006JD007219

Marshall, T. C., & Stolzenburg, M. (2001). Voltages inside and just above thunderstorms. *Journal of Geophysical Research*, *106*(D5), 4757–4768. https://doi.org/10.1029/2000JD900640

Montijn, C., Hundsdorfer, W., & Ebert, U. (2006). An adaptive grid refinement strategy for the simulation of negative streamers. *Journal of Computational Physics*, *219*, 801–835. https://doi.org/10.1016/j.jcp.2006.04.017

Morrill, W. L. (2000). Electron collision data for plasma chemistry modeling. *Advances In Atomic Molecular, and Optical Physics*, *43*, 79–110. https://doi.org/10.1016/S1049-250X(08)60122-6

Morrill, J. S., & Benesch, W. M. (1996). Auroral N_2 emissions and the effect of collisional processes on N_2 triplet state vibrational populations. *Journal of Geophysical Research*, *101*, 261–274. https://doi.org/10.1029/95JA02835

Moruzzi, J. L., Ekin, JrJ. W., & Phelps, A. V. (1968). Electron production by associative detachment of O^- ions with NO, CO, and H_2. *The Journal of Chemical Physics*, *48*, 3070–3076. https://doi.org/10.1063/1.1669574

Moudry, D., Stenbaek-Nielsen, H., Sentman, D., & Wescott, E. (2003). Imaging of elves, halos and sprite initiation at 1 ms time resolution. *Journal of Atmospheric and Solar-Terrestrial Physics*, *65*, 509–518. https://doi.org/10.1016/S1364-6826(02)00323-1

Nault, B. A., Nault, B. A., Laughner, J. L., Wooldridge, P. J., Crounse, J. D., Dibb, J., et al. (2017). Lightning NO_x emissions: Reconciling measured and modeled estimates with updated NO_x chemistry. *Geophysical Research Letters*, *44*, 9479–9488. https://doi.org/10.1002/2017GL074436

Neubert, T., Chanrion, O., Arnone, E., Zanotti, F., Cummer, S., Li, J., et al. (2011). The properties of a gigantic jet reflected in a simultaneous sprite: Observations interpreted by a model. *Journal of Geophysical Research*, *116*, A12329. https://doi.org/10.1029/2011JA016928

Neubert, T., Kuvvetli, I., Budtz-Jørgensen, C., Østgaard, N., Reglero, V., & Arnold, N. (2006). The atmosphere-space interactions monitor (ASIM) for the international space station. In *ILWS (International Living With a Star) Workshop*, Goa, India.

Newsome, R. T., & Inan, U. S. (2010). Free-running ground-based photometric array imaging of transient luminous events. *Journal of Geophysical Research*, *115*, A00E41. https://doi.org/10.1029/2009JA014834

Pagnon, D., Amorin, J., Nahorny, J., Touzeau, M., & Vialle, M. (1995). On the use of actinometry to measure the dissociation in O_2 DC glow discharges: Determination of the wall recombination probability. *Journal of Physics D: Applied Physics*, *28*, 1856–1868. https://doi.org/10.1088/0022-3727/28/9/014

Pancheshnyi, S. (2013). Effective ionization rate in nitrogen-oxygen mixtures. *Journal of Physics D: Applied Physics*, *46*, 155201. https://doi.org/10.1088/0022-3727/46/15/155201

Parra-Rojas, F. C., Luque, A., & Gordillo-Vázquez, F. J. (2013). Chemical and electrical impact of lightning on the Earth mesosphere: The case of sprite halos. *Journal of Geophysical Research: Space Physics*, *118*, 5190–5214. https://doi.org/10.1002/jgra.50449

Parra-Rojas, F. C., Luque, A., & Gordillo-Vázquez, F. J. (2015). Chemical and thermal impacts of sprite streamers in the Earth's mesosphere. *Journal of Geophysical Research: Space Physics*, *120*, 8899–8933. https://doi.org/10.1002/2014JA020933

Parra-Rojas, F. C., Passas, M., Carrasco, E., Luque, A., Tanarro, I., Simek, M., & Gordillo-Vázquez, F. J. (2013). Spectroscopic diagnostics of laboratory air plasmas as a benchmark for spectral rotational (gas) temperature determination in TLEs. *Journal of Geophysical Research: Space Physics*, *118*, 4649–4661. https://doi.org/10.1002/jgra.50433

Pasko, V. P., Inan, U. S., Taranenko, Y. N., & Bell, T. F. (1995). Heating, ionization and upward discharges in the mesosphere, due to intense quasi-electrostatic thundercloud fields. *Geophysical Research Letters*, *22*, 365–368. https://doi.org/10.1029/95GL00008

Pasko, V. P., Yair, Y., & Kuo, C.-L. (2012). Lightning related transient luminous events at high altitude in the Earth's atmosphere: Phenomenology, mechanisms and effects. *Space Science Reviews*, *168*, 475–516. https://doi.org/10.1007/s11214-011-9813-9

Passas, M., del Río, J. S., Luque, A., & Gordillo-Vázquez, F. J. (2014). Transient upper atmospheric plasmas: Sprites and halos. *IEEE Transactions on Plasma Science*, *42*(10), 2664–2665.

Passas, M., Sánchez, J., Sánchez-Blanco, E., Luque, A., & Gordillo-Vázquez, F. J. (2016). GRASSP: A spectrograph for the study of transient luminous events. *Applied Optics*, *55*(23), 6436–6442.

Pérez-Invernón, F. J., Gordillo-Vázquez, F. J., & Luque, A. (2016). On the electrostatic field created at ground level by a halo. *Geophysical Research Letters*, *43*, 7015–7222. https://doi.org/10.1002/2016GL069590

Pérez-Invernón, F. J., Luque, A., & Gordillo-Vázquez, F. J. (2016). Mesospheric optical signatures of possible lightning on Venus. *Journal of Geophysical Research: Space Physics*, *121*, 7026–7048. https://doi.org/10.1029/2016JA022886

Peverall, R., Rosen, S., Peterson, J. R., Larsson, M., Al-Khalili, A., Vikor, L., et al. (2001). Dissociative recombination and excitation of $O2^+$: Cross sections, product yields and implications for studies of ionospheric airglows. *Journal of Chemical Physics*, *114*, 6679–6689. https://doi.org/10.1063/1.1349079

Phelps, A. V. (1991). Cross sections and swarm coefficients for nitrogen ions and neutrals in N_2 and argon ions and neutrals in Ar for energies from 0.1 eV to 10 keV. *Journal of Physical and Chemical Reference Data*, *20*, 557. https://doi.org/10.1063/1.555889

Phelps, A. V. (2005). A compilation of atomic and molecular data: http://jila.colorado.edu/avp/

Phelps, V. (2008). NO electron cross sections: http://jilawww.colorado.edu

Piper, L. G. (1988). State-to-state $N_2(A\ ^3\sum_u^+)$ energy pooling reactions. II. The formation and quenching of $N_2(B\ ^3\Pi_g$, vscript=1-12). *Journal of Chemical Physics*, *88*, 6911–6921. https://doi.org/10.1063/1.454388

Piper, L. G. (1989). The excitation of $N_2(B^3\Pi_g$, v=1-12) in the reaction between $N_2(A^3\Sigma_u^+)$ and $N_2(X, v \geq 5)$. *Journal Chemical Physics*, *91*, 864–873. https://doi.org/10.1063/1.457138

Piper, L. G. (1992). Energy transfer studies on $N_2(X^1\Sigma_g^+, v)$ and $N_2(B^3\Pi_g)$. *Journal of Chemical Physics*, *97*, 270–275. https://doi.org/10.1063/1.463625

Piper, L. G., Green, B. D., Blumberg, W. A. M., & Wolnik, S. J. (1985). N_2^+ Meinel band quenching. *Journal of Chemical Physics*, *82*, 3139–3145. https://doi.org/10.1063/1.448211

Pitchford, L. C., McKoy, B. V., Chutjian, A., & Trajmar, A. (2012). Swarm studies and inelastic electron-molecule collisions. In *Swarm Studies and Inelastic Electron-Molecule Collisions: Proceedings of the Meeting of the Fourth International Swarm Seminar and the Inelastic Electron-Molecule Collisions Symposium, July 19–23, 1985*, Tahoe City, California, USA.

Price, C., Penner, J., & Prather, M. (1997). NO_x from lightning: 1. Global distribution based on lightning physics. *Journal of Geophysical Research*, *102*, 5929–5941. https://doi.org/10.1029/96JD03504

Qin, J., Pasko, V. P., McHarg, M. G., & Stenbaek-Nielsen, H. C. (2014). Plasma irregularities in the D-region ionosphere in association with sprite streamer initiation. *Nature Communications*, *5*, 3740. https://doi.org/10.1038/ncomms4740

Radzig, A. A., & Smirnov, B. M. (2012). *Reference data on atoms, molecules, and ions* (Vol. 31). Berlin, Heidelberg: Springer Science & Business Media.

Rakov, V. A., & Uman, M. A. (2003). *Lightning physics and effects*. Cambridge: Cambridge University Press.

Rodríguez, A. E., Morgan, W. L., Touryan, K. J., Moeny, W. M., & Martin, T. H. (1991). An air breakdown kinetic model. *Journal of Applied Physics*, *70*(4), 2015–2022. https://doi.org/10.1063/1.349487

Romps, D. M., Seeley, J. T., Vollaro, D., & Molinari, J. (2014). Projected increase in lightning strikes in the United States due to global warming. *Science*, *346*, 851–854. https://doi.org/10.1126/science.1259100

Schumann, U., & Huntrieser, H. (2007). The global lightning-induced nitrogen oxides source. *Atmospheric Chemistry and Physics*, *7*, 3823–3907. https://doi.org/10.5194/acp-7-3823-2007

Sentman, D. D., Stenbaek-Nielsen, H. C., McHarg, M. G., & Morrill, J. S. (2008). Plasma chemistry of sprite streamers. *Journal of Geophysical Research*, *113*, D11112. https://doi.org/10.1029/2007JD008941

Simek, M. (2002). The modelling of streamer-induced emission in atmospheric pressure, pulsed positive corona discharge: N_2 second positive and NO-γ systems. *Journal of Physics D*, *35*, 1967. https://doi.org/10.1088/0022-3727/35/16/311

Simek, M. (2003). Determination of $N_2(A\ ^3\Sigma_u^+)$ metastable density produced by nitrogen streamers at atmospheric pressure: 2. Experimental verification. *Plasma Sources Science and Technology*, *12*, 454. https://doi.org/10.1088/0963-0252/12/3/322

Skalni, J. D., Matejcik, S., Kiendler, A., Stamatovic, A., & Märk, T. D. (1996). Dissociative electron attachment to ozone using a high-resolution crossed beams technique. *Märk*, *255*, 112–118. https://doi.org/10.1016/0009-2614(96)00341-7

Slanger, T. G., & Copeland, R. A. (2003). Energetic oxygen in the upper atmosphere and the laboratory. *Chemical Reviews*, *103*(12), 4731–4766. https://doi.org/10.1021/cr0205311

Smirnov, B. M., & Massey, H. S. W. (1982). *Negative ions*: McGraw-Hill Companies.

Starikovskaia, S. M., Starikovskii, A. Y., & Zatsepin, D. V. (2001). Hydrogen oxidation in a stoichiometric hydrogen-air mixture in the fast ionization wave. *Combustion Theory Modelling*, *5*, 97–129.

Sweet, R. A. (1977). A cyclic reduction algorithm for solving block tridiagonal systems of arbitrary dimension. *SIAM Journal on Numerical Analysis*, *14*, 706–720.

Taranenko, Y. N., Inan, U. S., & Bell, T. F. (1993). The interaction with lower ionosphere of electromagnetic pulses from lightning: Excitation of optical emissions. *Geophysical Research Letters*, *20*, 2675–2678.

Thoman, J. J. W., Gray, J. A., Durant, J. J. L., & Paul, P. H. (1992). Collisional electronic quenching of $NO(A^2\Sigma^+)$ by N_2 from 300 to 4500 K. *Journal of Chemical Physics*, *97*, 8156. https://doi.org/10.1063/1.463437

Thomas, L. (1974). Recent developments and outstanding problems in the theory of the D region. *Radio Science*, *9*(2), 121–136.

Turnbull, D. N., & Lowe, R. P. (1991). Temporal variations in the hydroxyl nightglow observed during ALOHA-90. *Geophysical Research Letters*, *18*, 1345–1348. https://doi.org/10.1029/91GL01293

Vallance Jones, A. (1974). *Aurora*. Dordrecht, Holland: D. Reidel Publishing Co.

van der Velde, O. A., & Montanyà, J. (2016). Statistics and variability of the altitude of elves. *Geophysical Research Letters*, *43*, 5467–5474. https://doi.org/10.1002/2016GL068719

Viggiano, A. A. (2006). Much improved upper limit for the rate constant for the reaction of O2+ with N2. *The Journal of Physical Chemistry A*, *110*(41), 11,599–11,601. https://doi.org/10.1021/jp064962p

Watson, S. S., & Marshall, T. C. (2007). Current propagation model for a narrow bipolar pulse. *Geophysical Research Letters*, *34*, L04816. https://doi.org/10.1029/2006GL027426

Wescott, E. M., Stenbaek-Nielsen, H. C., Sentman, D. D., Heavner, M. J., Moudry, D. R., & Sabbas, F. T. S. (2001). Triangulation of sprites, associated halos and their possible relation to causative lightning and micrometeors. *Journal of Geophysical Research*, *106*, 10,467–10,477. https://doi.org/10.1029/2000JA000182

Whitaker, M., Biondi, M. S., & Johnsen, R. (1981). Electron-temperature dependence of dissociative recombination of electrons with N_2^+ N_2 dimer ions. *Physical Review A*, *24*, 743. https://doi.org/10.1103/PhysRevA.24.743

Wilson, C. T. R. (1925). The electric field of a thundercloud and some of its effects. *Proceedings of the Physical Society of London*, *37*, 32D.

Winkler, H., & Notholt, J. (2015). A model study of the plasma chemistry of stratospheric Blue Jets. *Journal of Atmospheric and Solar-Terrestrial Physics*, *122*, 75–85. https://doi.org/10.1016/j.jastp.2014.10.015

Yaron, M., von Engel, A., & Vidaud, P. (1976). The collisional quenching of O2*(1g) by NO and CO2. *Chemical Physics Letters*, *37*(1), 159–161. https://doi.org/10.1016/0009-2614(76)80186-8

Yee, K. S. (1966). Numerical solution of initial boundary value problems involving Maxwell's equations in isotropic media. *IEEE Transactions on Antennas and Propagation*, *14*, 302–307.

Zinn, J., Sutherland, C. D., & Ganguly, S. (1990). The solar flare of August 18, 1979—Incoherent scatter radar data and photochemical model comparisons. *Journal of Geophysical Research*, *95*, 16,705–16,718. https://doi.org/10.1029/JD095iD10p16705